Analysis of the biases in the downward shortwave surface flux in the GFDL CM2.1 general circulation model

Stuart M. Freidenreich[1] and V. Ramaswamy[1]

Received 23 August 2010; revised 5 January 2011; accepted 8 February 2011; published 22 April 2011.

[1] Simulations of downward shortwave surface fluxes by the coupled Geophysical Fluid Dynamics Laboratory (GFDL) CM2.1 general circulation model are compared against climatology derived from the Baseline Surface Radiation Network (BSRN), Global Energy Balance Archive, and International Satellite Cloud Climatology Project ISCCP-FD data sets. The spatial pattern of the model's biases is evaluated. An investigation is made of how these relate to accompanying biases in total cloud amount and aerosol optical depth and how they affect the surface temperature simulation. Comparing CM2.1's clear-sky fluxes against BSRN site values, for European, Asian, and North American locations, there are underestimates in the direct and overestimates in the diffuse, resulting in underestimates in the total flux. These are related to overestimates of sulfate aerosol optical depth, arising owing to the behavior of the parameterization function for hygroscopic growth of these aerosols at very high relative humidity. Contrastingly, flux overestimate biases at lower latitude locations are associated with underestimates in sea-salt and carbonaceous aerosol amounts. All-sky flux biases consist of underestimates for North America, Eurasia, southern Africa, and northern oceanic regions and overestimates for the Amazon region, equatorial Africa, off the west coast of the Americas, and southern oceanic regions. These biases show strong correlations with cloud amount biases. There are modest correlations of the flux biases with cool surface temperature biases over North America and Eurasia, warm biases over the Amazon region, and cool (warm) biases over the northern (southern) oceanic regions. Analyses assuming nonhygroscopicity illustrate that there is a reduction of surface temperature biases accompanying a reduction of sulfate aerosol optical depth biases, whereas a more significant improvement in the temperature simulation requires refining the model's simulation of cloudiness.

Citation: Freidenreich, S. M., and V. Ramaswamy (2011), Analysis of the biases in the downward shortwave surface flux in the GFDL CM2.1 general circulation model, *J. Geophys. Res.*, *116*, D08208, doi:10.1029/2010JD014930.

1. Introduction

[2] The downward solar flux at the surface is an important component of the Earth's climate system. The exchange of energy between the surface and atmosphere is a major factor in governing the surface temperature and hydrologic cycle. In turn, it affects other physical processes at the surface, such as those involving sea ice and vegetation. There is evidence of climatic changes due to perturbations in the solar irradiance (e.g., by aerosols [*Forster et al.*, 2007]). Evidence of possible decadal variations in solar surface radiation [*Wild*, 2009] has brought attention to its influence on the surface heat budget. Reliable ground-based observations or satellite-derived estimations of the surface flux climatology are a prerequisite for establishing the quantitative changes in the heat and moisture budgets, and, thus, for understanding changes in surface climate. These are also essential for properly assessing model biases in the surface irradiance, and in the analysis of the atmospheric factors (aerosols, clouds, and water vapor) affecting the flux determination. The analysis of these biases provides the basis to identify shortcomings in models and offer a means by which GCM simulations can be tested, verified and further improved through appropriate modifications of the parameterizations.

[3] Earlier comparison studies had noted an overestimate of surface solar irradiance in GCMs [*Garratt*, 1994; *Wild et al.*, 1995; *Arking*, 1996; *Zhang et al.*, 1998]. *Wild and Liepert* [1998] attributed this to an underestimate of shortwave absorption in the atmosphere. The cause of this has been attributed to the rudimentary treatment in GCMs of the absorption properties of clouds [*Cess et al.*, 1995]. Other causes that have been speculated include the simulation of absorbing aerosol (or its absence entirely), and the underestimation of the contribution of water vapor absorption, due to the use of outdated spectroscopic databases forming the basis for its parameterization [*Wild*, 1999]. *Wild et al.* [2006] further demonstrated that inclusion of aerosols was a significant factor in reducing the annual mean clear-sky flux bias between modeled and Baseline Surface Radiation

[1]Geophysical Fluid Dynamics Laboratory, NOAA, Princeton University, Princeton, New Jersey, USA.

0148-0227/11/2010JD014930

Network (hereinafter BSRN) observed climatology averaged among several GCMs participating in the IPCC 2007 Assessment Report. A review of the evaluation of surface radiation budgets in GCMs is given by *Wild* [2008].

[4] The distinctive features of the GFDL CM2 coupled model [*Delworth et al.*, 2006] afford an investigation of these issues on a more solid footing. The model includes the following features: (1) all the important aerosol types (i.e., sulfate, carbonaceous, dust, and sea salt) are accounted for, (2) fully prognostic scheme is used for determining cloud amount and its radiative properties, (3) multiband solar parameterization accounts for the spectral dependence of scattering and absorption by clouds and aerosols, and (4) water vapor parameterization is used that is based on a version of the line parameter catalog, specifically HITRAN 2000 [*Rothman et al.*, 2003], that is more updated than that guiding some of the earlier studies. In comparison with previous GCM studies utilizing clear-sky BSRN data [e.g., *Wild et al.*, 2006], the GFDL model is used to conduct a more in-depth analysis of the relationship of aerosol optical depth and downward shortwave flux biases. Also, as part of this endeavor, the separate contributions of the direct and diffuse components in this relationship are examined. Similar to the work of *Bodas-Salcedo et al.* [2008], both ground-based and satellite-based flux data sets are used to assess GCM all-sky shortwave surface flux biases and their association with cloud amount and surface temperature. In this study, more of a focus is placed on explicitly quantifying their spatial relationships and seasonal dependencies.

2. Model Characteristics

[5] For this study, results are obtained from experiments performed with version 2.1 of the coupled GFDL GCM (hereinafter referred to as CM2.1). The characteristics of the atmosphere/land portion of the GCM are described by *Anderson et al.* [2004], while the remaining details regarding the ocean physics and its coupling to the atmosphere appears in the work of *Delworth et al.* [2006]. Some of the characteristics of the atmospheric model that are pertinent to the determination of the surface flux and its comparison with the observed and estimated climatology are highlighted here.

[6] The horizontal resolution of the GCM is 2.5 by 2 degrees. To compare with the climatology derived from ground-based measurements at site locations in continental interiors, the model flux values at the four surrounding grid points are linearly interpolated to the latitude and longitude of a site, to define the comparable model value at that point. Among the sites, there are several island locations that are not resolved as land, but are treated entirely as ocean in the model. For these too, the four-point interpolation scheme is used. For coastal site locations where there are land and ocean characteristics among the surrounding grid points (mainly with regards to the model's simulated surface albedo), the one that has the largest fraction of land characteristics, and is nearest to the site, is chosen to represent the model's site flux value.

[7] The shortwave radiation parameterization divides the solar spectrum into 18 bands (5 near-infrared, 4 visible, and 9 ultraviolet). The delta-Eddington technique [*Joseph et al.*, 1976] is used to compute layer reflection and transmission, and an adding technique [*Ramaswamy and Bowen*, 1994] is used to combine the vertically inhomogeneous atmosphere. The diffuse incident beam is assumed to be isotropic, with an effective zenith angle of 53 degrees. Further details regarding the development of the solar radiation parameterization are described by *Freidenreich and Ramaswamy* [1999], with updates described by *Freidenreich and Ramaswamy* [2005]. The radiation time step is 3 h. Mass concentrations for sulfate, carbonaceous and dust aerosols are derived from the MOZART-2 three-dimensional chemical transport model [*Horowitz*, 2006; *Horowitz et al.*, 2003], and the time evolution of monthly mean aerosol amounts is prescribed based on MOZART-2 simulations [*Ginoux et al.*, 2006]. Water drop and ice optical properties follow the *Slingo* [1989] and *Fu and Liou* [1993] formulations, respectively.

[8] The climate model results, that are the main focus of this study, consist of an ensemble of five coupled experiments. These experiments cover the time period from 1860 to 2003, but the model results used for comparisons here are mainly confined to the time periods of the reference data sets. Another ensemble of three experiments generated with the CM2.1 model configuration is also utilized, in which the sulfate aerosol optical properties are constrained to be nonhygroscopic (dry sulfate).

3. Data and Analysis Strategy

[9] The BSRN flux database consists of very high frequency (time resolution is mostly 1 min intervals) measurements of both shortwave and longwave components, at a relatively limited number of sites. The database was established in the early 1990s, and data collection continues to the present. The downward shortwave flux data consist of separate measurements of the direct, diffuse and total components, although the total is preferentially determined by summing the direct and diffuse measurements. Further details regarding the network, such as technical specifications, measuring techniques and archiving of data, can be found in the work of *Ohmura et al.* [1998]. The data set is a particularly useful tool to derive reliable estimates of the clear-sky shortwave irradiance at the surface. The fine temporal resolution allows for the detection of periods when clear skies were likely present, on the basis of the fact that cloudy skies exhibit unique shortwave characteristics, both instantaneously and when averaged over short periods of time. This feature has been used to construct a detection algorithm [*Long and Ackerman*, 2000], and this is applied to the BSRN database to obtain daily mean clear-sky surface flux estimates. As discussed in that study and reiterated by *Zhang et al.* [2010], virtually any bias in the clear-sky estimates comes from the measurements themselves rather than the detection algorithm used to produce them. The uncertainties associated with individual shortwave measurements are about 2 W/m^2 for the direct, and 5 W/m^2 for the diffuse and total irradiances. These are further reduced when averaging the daily estimates to obtain monthly means. The resultant monthly mean clear-sky (as well as all-sky) direct, diffuse and total flux values have been provided by C. Long and are obtained from the NASA Langley Research Center, through its Atmospheric Sciences Data Center's Global Energy and Water Cycle Experiment (GEWEX) Web site (http://gewex-rfa.larc.nasa.gov). Figure 1

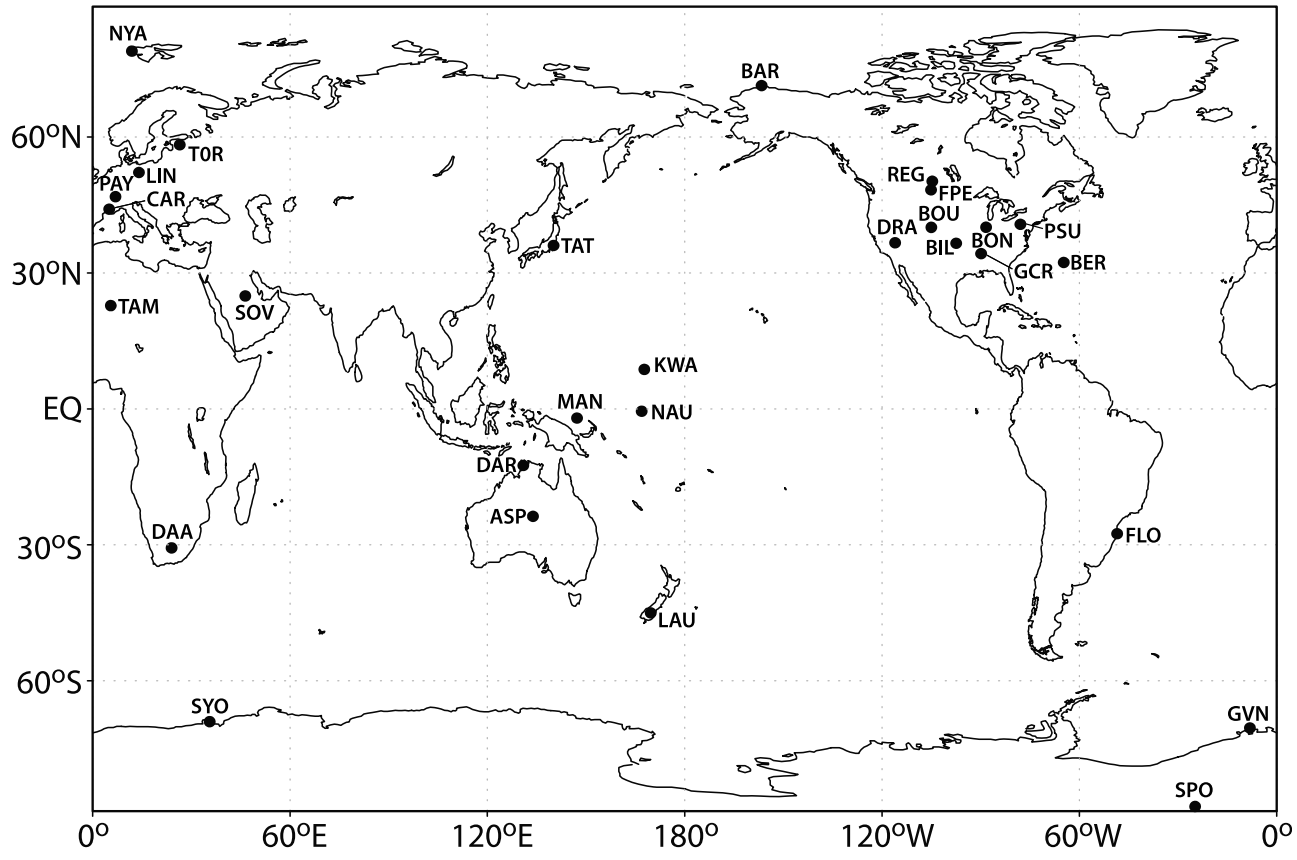

ASP Alice Springs, Australia
BAR Barrow, Alaska
BER Bermuda Island
BIL Billings, Oklahoma
BON Bondville, Illinois
BOU Boulder, Colorado
CAR Carpentras, France
DAR Darwin, Australia
DAA De Aar, South Africa
DRA Desert Rock, Nevada
FLO Florianopolis, Brazil
FPE Fort Peck, Montana
GVN Georg von Neumayer, Antarctica
GCR Goodwin Creek, Mississippi
KWA Kwajalein Island
LAU Lauder, New Zealand
LIN Lindenberg, Germany
MAN Manus, Papua New Guinea
NAU Nauru Island
NYA Ny Alesund, Spitsbergen
PAY Payerne, Switzerland
PSU Rock Springs, Pennsylvania
REG Regina, Saskatchewan
SOV Solar Village, Saudi Arabia
SPO South Pole, Antarctica
SYO Syowa, Cosmonaut Sea
TAM Tamanrasset, Algeria
TAT Tateno, Japan
TOR Toravere, Estonia

Figure 1. The identifiers and locations of the BSRN sites used in this study.

displays the location of the sites considered in this study; for each a clear-sky climatology has been derived. For comparison with BSRN, the model climatology is obtained by averaging the results for the same period through 2003 (the last year of the model integration).

[10] The clear-sky climatology is used to analyze the effects of atmospheric clear-sky composition on the simulated downward surface flux bias. The direct, diffuse and total components are analyzed separately. The two primary constituents in this respect are essentially aerosols and water vapor. It is hypothesized that the sign and magnitude of the bias between the model simulation and the BSRN climatology is mainly associated with the uncertainty in aerosol optical depth; however, the possible uncertainty in the flux due to water vapor uncertainty is also explored. Comparison with the diffuse flux climatology is also useful for unraveling large model biases in surface albedo. In this study, this is used to identify the deficiencies in the model's determination of sea ice.

[11] The all-sky climatology is mainly used to assess similarities in the model biases with respect to other flux data sets (described below). It is also used to establish a

linkage between model biases in the flux and in the total cloud amount (or equivalently the cloud cover fraction). *Long et al.* [2006] discuss a technique for estimating daily cloud amount from high temporal resolution flux measurements; the resulting estimate agrees to better than 10% with the corresponding observed value. This technique has been applied to the BSRN observations, and the resulting monthly mean values used in this assessment are obtained from the GEWEX Web site.

[12] International Satellite Cloud Climatology Project (hereinafter ISCCP-FD) (D2 version) is a global, satellite-based data set [*Zhang et al.*, 2004]. Available climatology of the all-sky downward surface flux and total cloud amount from this data set are utilized in this study. The flux values are obtained from the GEWEX Web site, while the cloud amount values are obtained from the ISCCP Web site (http://isccp.giss.nasa.gov). The uncertainty is estimated to be 10–15 W/m^2 for the surface flux components [*Zhang et al.*, 2004], with a substantial portion of this arising from errors in the input quantities, and not from the radiative transfer model used for the flux calculations [*Zhang et al.*, 2010]. *Zhang et al.* [2010] also found that the ISCCP-FD product effectively incorporates aerosol optical depth values that are too large by about a factor of 2. Thus, its clear-sky total shortwave flux estimates are biased lower, and this affects the all-sky values as well. This feature may have an effect on the model comparisons for regions of high aerosol concentrations. From *Rossow and Schiffer* [1999], the uncertainty in the estimated cloud amounts is 5%, except in the summertime polar regions where these may be ~10%. In this study, the biases in the ISCCP-FD cloud amounts are further highlighted, by comparing them with the Long-estimated values. With respect to the analysis of CM2.1's biases, the ISCCP-FD climatology is used in the following ways: (1) as a verification tool for checking consistencies in the sign and magnitude of the flux differences between CM2.1 and the ground-based measurements, (2) to determine CM2.1's flux biases in regions where ground-based data are sparse or nonexistent (mainly oceanic regions), (3) to assess the regional relationship of CM2.1's flux biases with corresponding biases in cloud amount, and (4) to assess the regional relationship of CM2.1's flux biases with corresponding biases in surface temperature (a separate data set is used and is described below). The monthly and seasonal mean differences are analyzed for the period (1984–2003), when the first full year of ISCCP-FD data availability overlaps with the model's integration.

[13] Global Energy Balance Archive (hereinafter GEBA) data provided by the Swiss Federal Institute of Technology are obtained from the Web site (http://www.iac.ethz.ch). It consists of a monthly mean all-sky flux climatology derived from pyranometer measurements made at over 1000 sites, for varying time periods. The relative random error of the monthly and annual mean is estimated to be approximately 5% and 2%, respectively [*Gilgen et al.*, 1998]; monthly and seasonal mean values are utilized in this study. It is also used to verify consistencies in the sign and magnitude of the model flux biases among the various data sets; it further provides another tool for investigating the linkage of CM2.1's flux biases with corresponding biases in cloud amount and surface temperature. The model climatology is based on the same period as the data available for each site.

[14] Three other data sets are utilized to investigate the linkage of the model's flux biases to those in other quantities. The Aerosol Robotic Network (AERONET) [*Holben et al.*, 2001] monthly mean climatology is obtained from the Web site (http://aeronet.gsfc.nasa.gov), and is used to quantify the model's aerosol optical depth bias. The data are based on direct measurements of aerosol optical depth. Since the instruments are well calibrated and the data are screened for clouds, the precision reaches 0.01. National Center for Environmental Prediction (NCEP) reanalysis of monthly water vapor profiles are obtained from the Website (http://www.esrl.noaa.gov), and are used to estimate the uncertainty in the clear-sky flux due to water vapor uncertainty. European Centre for Medium-Range Weather Forecasts (ECMWF) ERA-40 monthly temperature data are obtained from the Web site (http://data.ecmwf.int/data), and is used to investigate the model's surface temperature bias and its relationship with the corresponding flux bias, for monthly and seasonal time scales. Note that the surface temperature differences are analyzed for the same base period (1984–2003) used for the model comparisons with ISCCP-FD data.

4. Results

4.1. Clear-Sky (BSRN)

[15] The difference in the clear-sky direct, diffuse and total (direct+diffuse) surface flux components between the model and BSRN are first analyzed. Figures 2–4 illustrate the difference in the monthly mean direct, diffuse and total values, respectively, with and without aerosols included in the model. A subset of the BSRN sites shown in Figure 1 are selected for which aerosol optical depth or surface albedo play a key role in the results. Further, in order to examine their relationship with the biases in aerosol optical depth, Figure 5 illustrates the corresponding monthly mean values from the model and from AERONET climatology (except for the two Antarctic sites). Some of the AERONET locations chosen are in the same vicinity as BSRN, but if one is not available, or if one with a more complete monthly climatology is available nearby, then that location is chosen.

[16] From Figure 2, there are overestimates of the BSRN direct values for all months and at all site locations when aerosols are excluded. Maximum differences greater than 30 W/m^2 occur at most of the site locations. Likewise, from Figure 3, the model consistently underestimates the observed diffuse flux values when aerosols are excluded, with maximum differences greater than 20 W/m^2. From Figure 4, there is a resulting overestimate in the total flux value at most of the sites. Such differences indicate that the presence of an absorbing+scattering constituent (such as aerosols) is needed to impart more realism to the model simulation. These results also indicate, to some extent, the magnitude of the aerosol optical depth needed to be simulated by the model, in order to bring the direct, diffuse and total flux more in line with the observed at these locations. Thus, the sites for Europe, Asia and North America all have significant flux differences in tandem with observed aerosol optical depths >0.1 (Figure 5). Further, the sites with the largest (Solar Village and Tamanrasset) and smallest (Lauder and Nauru Island) flux differences in the absence of aerosols are accompanied by relatively large and small observed aerosol optical depths, respectively.

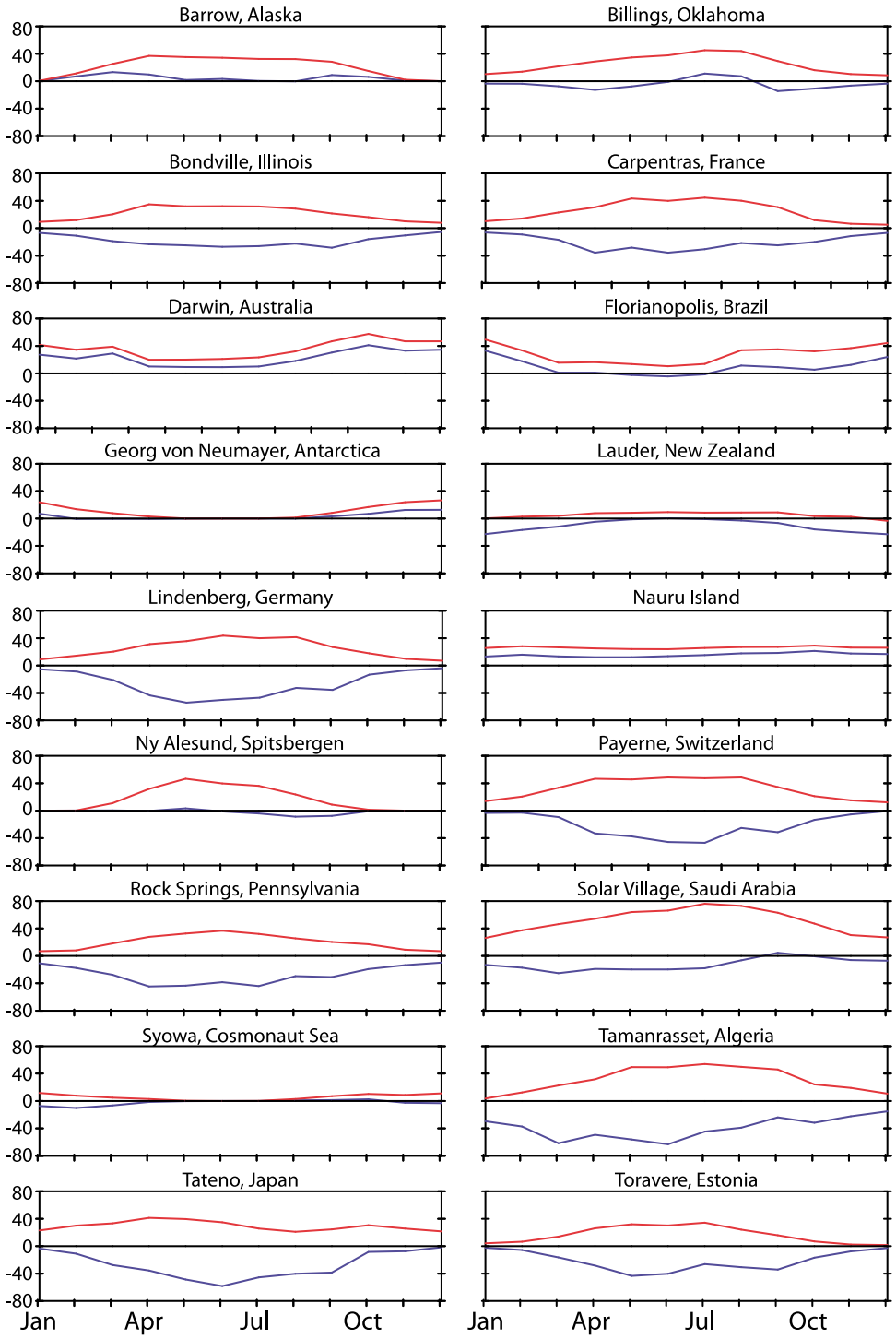

Figure 2. The difference in the monthly mean, direct downward clear-sky surface flux (W/m^2) between CM2.1 and BSRN for various site locations. Results are presented with aerosols (blue lines) and without aerosols (red lines) included in the model simulation.

[17] The flux differences with BSRN when aerosols are included in the model, and how they relate to differences between the modeled and observed aerosol optical depths, are next analyzed. Specifically, this is to assess whether an overestimate (underestimate) in the direct and an underestimate (overestimate) in the diffuse flux can be associated with an underestimate (overestimate) in the aerosol optical depth. The model locations corresponding to the European (Carpentras, Lindenberg, Payerne and Toravere), Asian (Tateno), Saharan desert (Tamanrasset) and eastern U.S. (Bondville and Rock Springs) sites all display a significant underestimate in the direct and an overestimate in the diffuse flux for all months (maximum values >40, 20 W/m^2, respectively) when aerosols are included. Consistent with

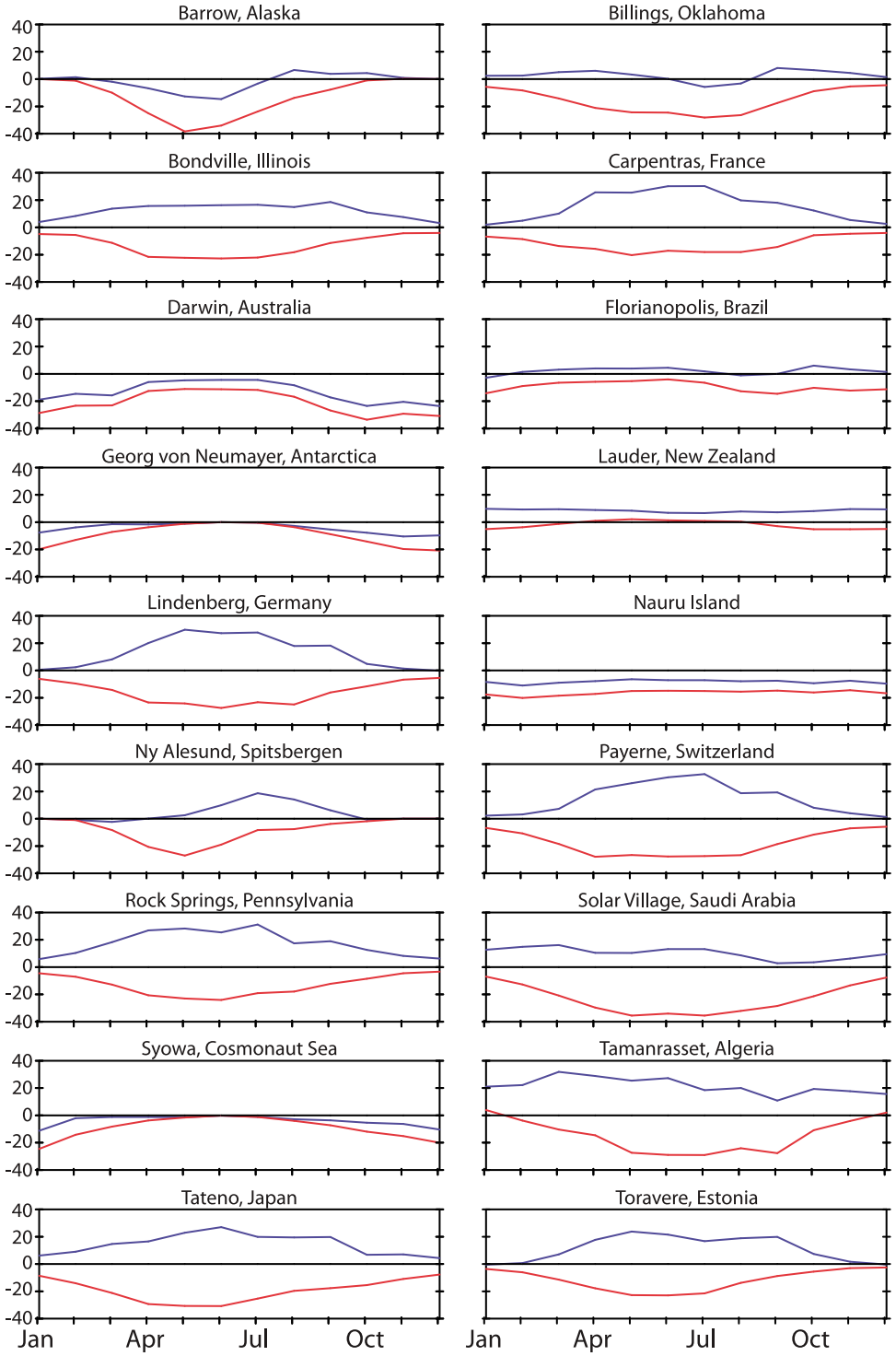

Figure 3. Same as Figure 2 except for the diffuse flux.

these findings, Figure 5 shows that the model overestimates the AERONET climatological values of aerosol optical depths at or near these locations. Contrastingly, the flux differences at Darwin, Florianopolis and Nauru Island are similar in sign but reduced in magnitude with respect to the case without aerosols included. This implies an underestimate of the observed aerosol optical depth, and Figure 5 shows that this occurs. For Billings, the sign of the flux bias is consistent with the greater overestimation of aerosol optical depth that occurs in the spring and autumn. Compared with other site locations with a relatively large aerosol optical depth present, Solar Village shows the smallest bias in both the simulated flux and aerosol optical depth. Thus, these two site locations illustrate that the linkage between clear-sky flux and aerosol optical depth biases is evident when looking at the finer details as well. Except for polar

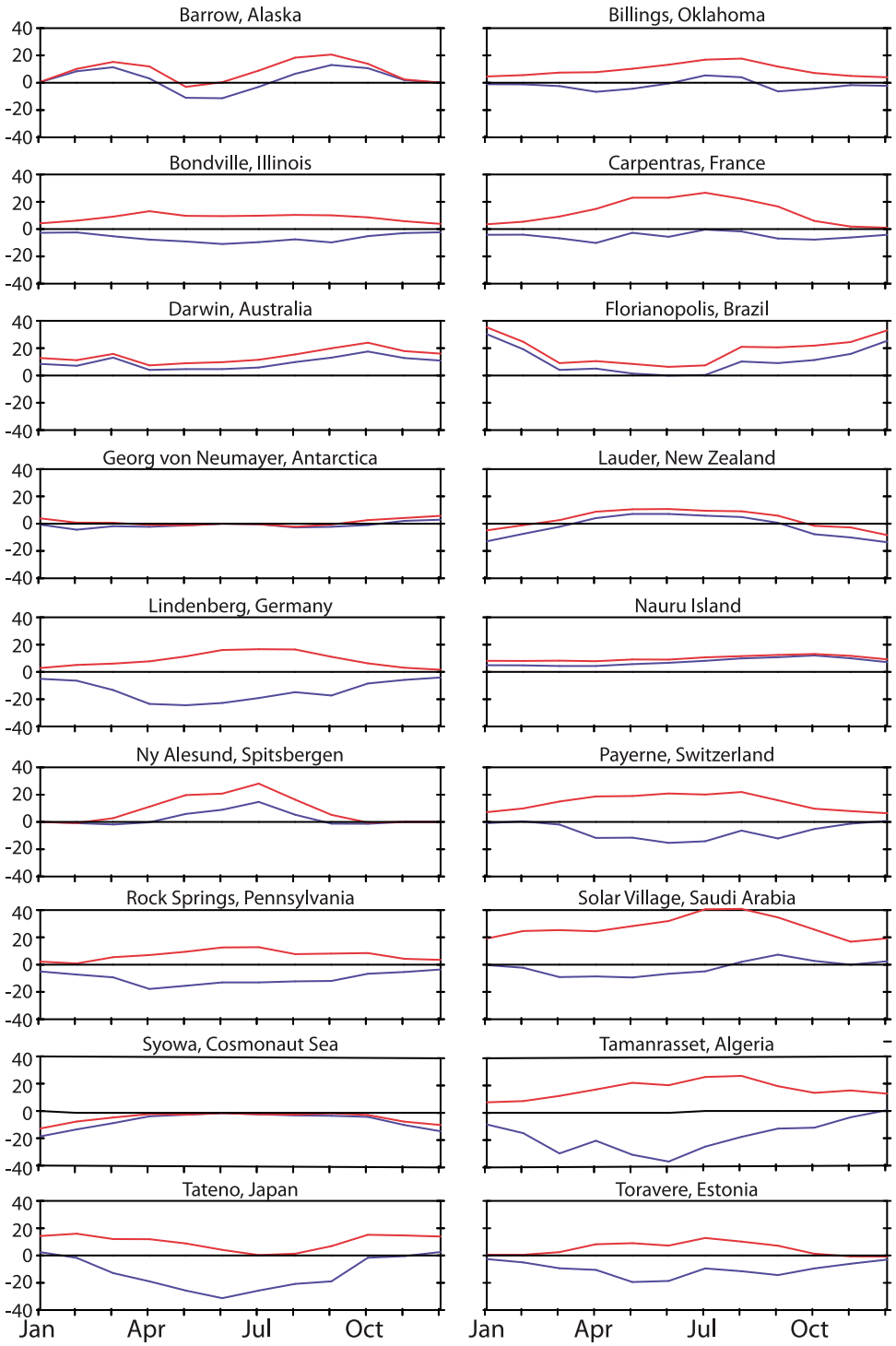

Figure 4. Same as Figure 2 except for the total (direct plus diffuse) flux.

site locations, the sign of the difference in the total flux is similar to what is seen for the direct component, thus showing the dominance of this component. For the polar site locations, a higher surface albedo enhances the contribution of the diffuse component.

[18] Biases can also arise from the modeling of water vapor absorption, and these could affect the attribution of the clear-sky flux biases to solely aerosol optical depth. The errors in the case of water vapor arise from its parameterization (say, in comparison with benchmark line-by-line computations), and from differences between simulated and actual water vapor profiles. From *Freidenreich and Ramaswamy* [1999, Table 7], the error in the parameterized total clear-sky downward flux with respect to line-by-line benchmark computations is found to be about 1%, mostly owing to water vapor (similar errors are present in

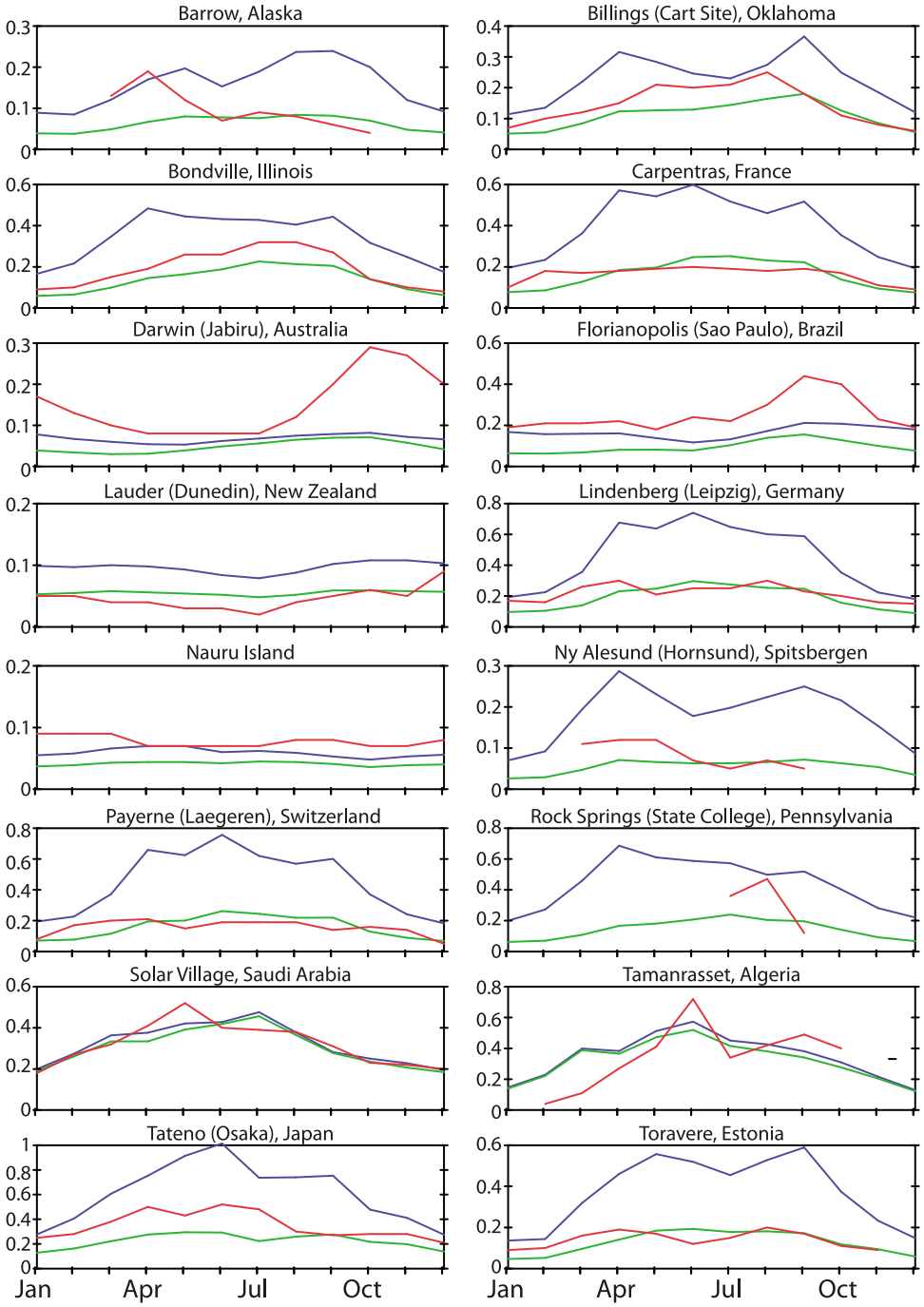

Figure 5. The monthly mean aerosol optical depth from CM2.1 (blue lines) and AERONET (red lines) for various AERONET site locations. Also illustrated are the model results from an ensemble of experiments (green lines) that assume "dry" sulfate (see section 4.3). Locations chosen are the same as either BSRN or a nearby area, with the corresponding AERONET site location indicated in parentheses.

the revised parameterization used in this study). Applying to this estimate the annual mean flux values determined at the BSRN locations (see Table 1) translates into a maximum error of <3 W/m^2. In order to estimate the error contribution due to water vapor profiles, monthly mean values from the model and from NCEP reanalysis estimates for the same time period are applied to a standalone version of the GCM. Globally, maximum differences in the annual mean downward surface flux of about 10 W/m^2 occur, but, at the BSRN locations, these are <3 W/m^2. Although the NCEP data can also have uncertainties, these flux uncertainties are considerably less than the flux overestimates that result when aerosols are excluded from consideration in the model. They are also significantly less than the flux underestimates that result when aerosols are included, particularly at the BSRN locations where they contribute significantly to the depletion

Table 1. Annual Mean, Downward Clear-Sky Shortwave Flux (W/m^2) at the Surface From BSRN for the Direct, Diffuse, and Total Components, and the Corresponding Differences With CM2.1[a]

Site	BSRN			CM2.1 - BSRN		
	Direct	Diffuse	Total	Direct	Diffuse	Total
Alice Springs	260.7	30.9	291.7	−6.7	3.3	−3.5
Barrow	108.1	30.3	138.4	0.1	−2.9	−2.8
Bermuda	220.3	36.4	256.7	−3.5	−1.2	−4.7
Billings	212.8	38.4	251.2	−8.4	1.8	−6.6
Bondville	204.7	35.6	240.3	−22.4	11.1	−11.4
Boulder	218.6	31.2	249.8	−5.5	2.8	−2.7
Carpentras	187.4	33.0	220.4	−25.6	14.1	−11.5
Darwin	245.5	46.7	292.3	22.5	−13.6	8.9
De Aar	247.6	25.6	273.2	−5.6	6.7	1.1
Desert Rock	230.4	32.3	262.7	−1.4	0.3	−1.1
Florianopolis	231.9	32.7	264.6	4.7	1.5	6.2
Fort Peck	182.4	31.7	214.1	−5.3	1.3	−4.0
Georg Von Neumayer	123.3	30.8	154.1	4.3	−4.2	0.1
Goodwin Creek	212.6	38.6	251.2	−9.3	4.9	−4.4
Kwajalein	257.0	38.0	295.0	7.7	−6.2	1.5
Lauder	211.3	22.3	233.6	−11.9	8.2	−3.7
Lindenberg	158.2	36.2	194.4	−31.3	11.5	−19.7
Manus	259.7	39.2	298.9	6.8	−5.5	1.3
Nauru Island	259.7	39.0	298.7	14.6	−8.3	6.2
Ny Alesund	96.6	28.2	124.8	−5.4	2.6	−2.8
Payerne	175.2	37.7	212.9	−26.2	12.9	−13.3
Regina	179.1	32.3	211.5	−9.4	0.3	−9.0
Rock Springs	206.4	35.5	241.9	−33.4	15.7	−17.7
Solar Village	229.8	50.8	280.5	−15.0	9.4	−5.6
South Pole	119.3	23.5	142.9	2.1	−2.0	0.1
Syowa	129.6	29.6	159.2	2.0	−3.1	−1.1
Tamanrasett	255.1	41.3	296.4	−40.2	21.3	−18.8
Tateno	214.1	41.3	255.3	−36.1	11.8	−24.3
Toravere	144.7	30.7	175.4	−26.8	9.3	−17.5

[a]Total components equal direct plus diffuse. For comparison with BSRN, the model climatology is obtained for the same period as when data are available for each site location through 2003 (the last year of the model integration).

of the incoming solar irradiance (see Table 1). Thus, water vapor biases do not impact the flux biases appreciably, nor the interpretation of the effect of flux biases on the clear-sky comparisons, particularly at locations where they are principally attributable to aerosol optical depth.

[19] The contributing factors toward CM2.1's biases of the aerosol optical depth in various regions have been analyzed in detail [see *Ginoux et al.*, 2006]. They are briefly highlighted here with respect to the BSRN/AERONET locations, in order to explain the resulting differences noted in Figure 5. For Europe, eastern Asia and North America, hygroscopic sulfate is the primary component of the total aerosol optical depth. Also, in CM2.1, there exists a moist bias at and near the surface. For example, examination of ECMWF ERA-40 monthly mean relative humidity climatology indicates values of 60–70% are common in these areas, but CM2.1 produces values exceeding 80%. Upon closer examination, it is found that CM2.1's daily mean relative humidity frequently reach 100% for these regions. Further, hygroscopic growth of sulfate aerosols is assumed to occur for relative humidity all the way up to 100%. The overestimate in aerosol optical depth arises because of the nature of the parameterization expression at very high relative humidity, particularly for values in excess of ~95%. The increase in aerosol extinction with relative humidity is especially large at these values [*Haywood and Ramaswamy*, 1998]. For instance, it approximately doubles from 95% to 98%, and increases further by more than a factor of 3 from 98% to 100%. This causes the magnitudes of the monthly mean biases in the simulated aerosol optical depths, and of the attendant depletion of the clear-sky solar irradiance, for the pertinent BSRN/AERONET locations, to be skewed toward greater values than the bias in the corresponding relative humidity mean alone would imply. CM2.1 also does not account well for the presence of carbonaceous aerosols in regions of biomass burning, such as the Amazon, which maximizes during the summer and autumn seasons. As a result, Figure 5 shows the largest underestimation in aerosol optical depth occurring for Florianopolis/Sao Paulo during this time. Further, sea-salt concentrations are underestimated by more than a factor of 2 globally in CM2.1, and its optical depth is up to half of the total value for the western tropical Pacific. This contributes toward the underestimate seen for Nauru Island. Thus, improvements in the treatment of the parameterization of sulfate's hygroscopicity, and better determination of carbonaceous and sea-salt aerosol concentrations, are needed to reduce the biases noted in Figures 2–5. In section 4.3, how a reduction of sulfate aerosol optical depth impacts the model's simulation of surface temperature will be explored.

[20] The BSRN clear-sky diffuse flux climatology is also a useful diagnostic for unraveling the large model biases in surface albedo. For CM2.1, it is used to confirm deficiencies noted previously in the determination of sea ice [*Delworth et al.*, 2006]. CM2.1's sea ice is found to grow too early and then melt too rapidly in the Northern Hemisphere, while its geographical extent is too small in the Southern Hemisphere. These attributes affect the simulated surface albedo, and the corresponding diffuse flux scattered back down to the surface. The differences for four of the polar site locations (Barrow, Ny Alesund, Georg von Neumayer and Syowa; see Figure 1) are illustrated in Figure 3. After accounting for aerosols, both Arctic site locations (Barrow and Ny Alesund) show an overestimate of the diffuse flux occurring during the late summer and autumn months; Barrow shows an underestimate during the spring and early summer months. The Antarctic locations (Georg von Neumayer and Syowa) show a more consistent underestimate. These characteristics are thus in tandem with the aforementioned sea-ice deficiencies.

[21] Table 1 summarizes the BSRN annual mean direct, diffuse and total clear-sky flux values, and the differences with CM2.1, for the site locations already considered above, as well as the remaining ones shown in Figure 1. The sites exhibiting the largest total clear-sky underestimates, >10% of the reference value (e.g., Lindenberg, Tateno, Toravere), are an indication of the clear-sky direct aerosol effects on the shortwave radiation budget, and the degree to which the modeling of aerosol extinction needs to be improved. The remaining North American sites not considered in the previous analysis (Bermuda, Boulder, Desert Rock, Fort Peck, Goodwin Creek) display somewhat smaller underestimates. There are flux overestimates at Kwajalein and Manus, which are near Nauru Island (Figure 1), an indication of a similar aerosol bias endemic to that region. The agreement in the total flux is quite good for the polar sites despite any diffuse flux discrepancies.

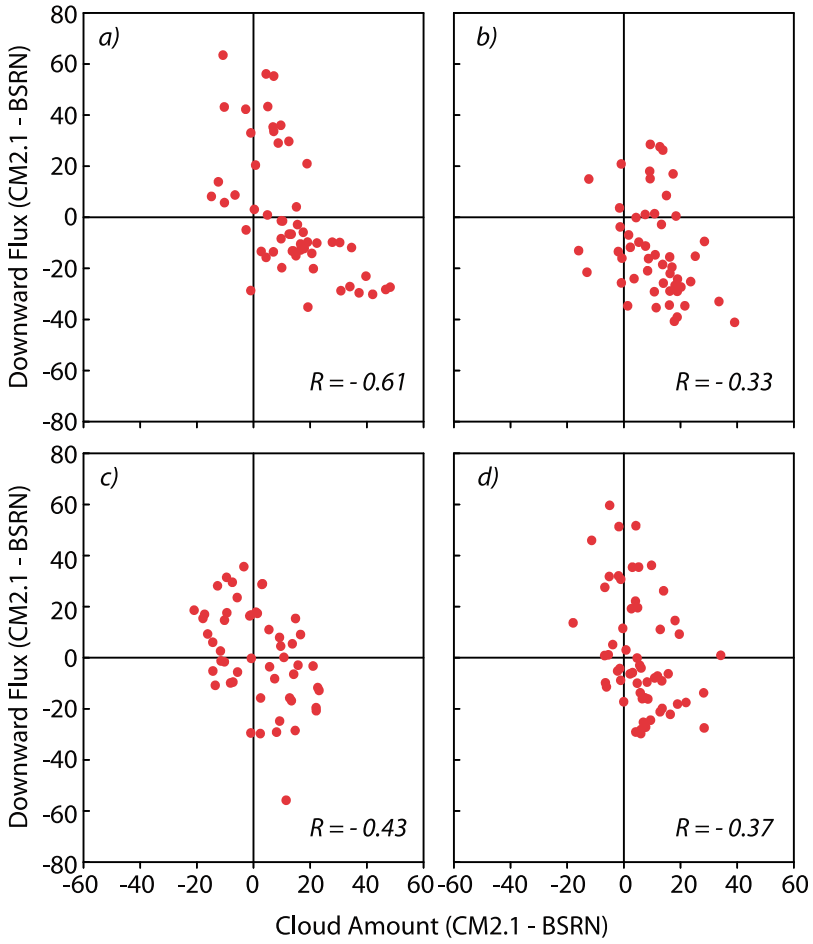

Figure 6. The relationship of the time mean CM2.1 minus BSRN downward all-sky surface flux (W/m^2) and the CM2.1 minus Long-estimated total cloud amount (%) derived from the BSRN data for (a) December plus January plus February, (b) March plus April plus May, (c) June plus July plus August, and (d) September plus October plus November. Also shown is the pattern correlation coefficient R.

4.2. All-Sky (BSRN, GEBA, and ISCCP-FD)

[22] Previous assessments of the simulation characteristics for both CM2.1 [*Delworth et al.*, 2006], and the corresponding atmospheric/land model with prescribed SSTs [*Anderson et al.*, 2004], have been limited in scope in analyzing the all-sky shortwave flux biases, their relationship with cloud amount, and their effect on the simulated surface temperature. In this study, the CM2.1's all-sky flux biases at the surface are explicitly quantified, in contrast to merely the shortwave atmospheric absorbed flux explored in the earlier studies. Additionally, how they relate to biases in the modeled cloud amount, and in turn, the global surface temperature simulation, is determined.

[23] Similarities in the sign and magnitude of the GCM's flux biases among the BSRN, GEBA and ISCCP-FD data sets are sought, in order to establish the regional dependencies among the key variables. However, for regions where ground-based data are particularly sparse or nonexistent (especially oceanic locations), results that arise from comparisons with the ISCCP-FD data set alone are considered. The linkages between the flux biases in particular regions to those occurring in cloud amounts are investigated. The ISCCP-FD flux and cloud amount data are used together as a reference for quantifying the regional pattern of this relationship. However, several intermediate comparisons are necessary in order to add a greater measure of certainty to this type of analysis.

[24] First, to get an overview of the linkage, model biases are assessed using the BSRN flux and the Long-estimated cloud amount climatology. These are directly related to the downwelling radiation measurements made at the BSRN sites, and offer the most direct assessment of this linkage. Figure 6 illustrates the monthly mean differences partitioned into the various seasons. There is a modest negative correlation (about −0.3 to −0.6) between them; that is, larger model overestimates (underestimates) of the flux are generally associated with larger underestimates (overestimates) in the corresponding cloud amounts. Thus, the degree of the model bias in cloud amount becomes an important factor governing the associated bias in the downward all-sky flux at the surface.

[25] Second, a broader geographical perspective is given to this linkage, by analyzing the model biases with respect to the GEBA flux and the ISCCP-FD cloud amount climatology. The analysis is limited to sites in continental interiors (for consistency with similar comparisons made with the

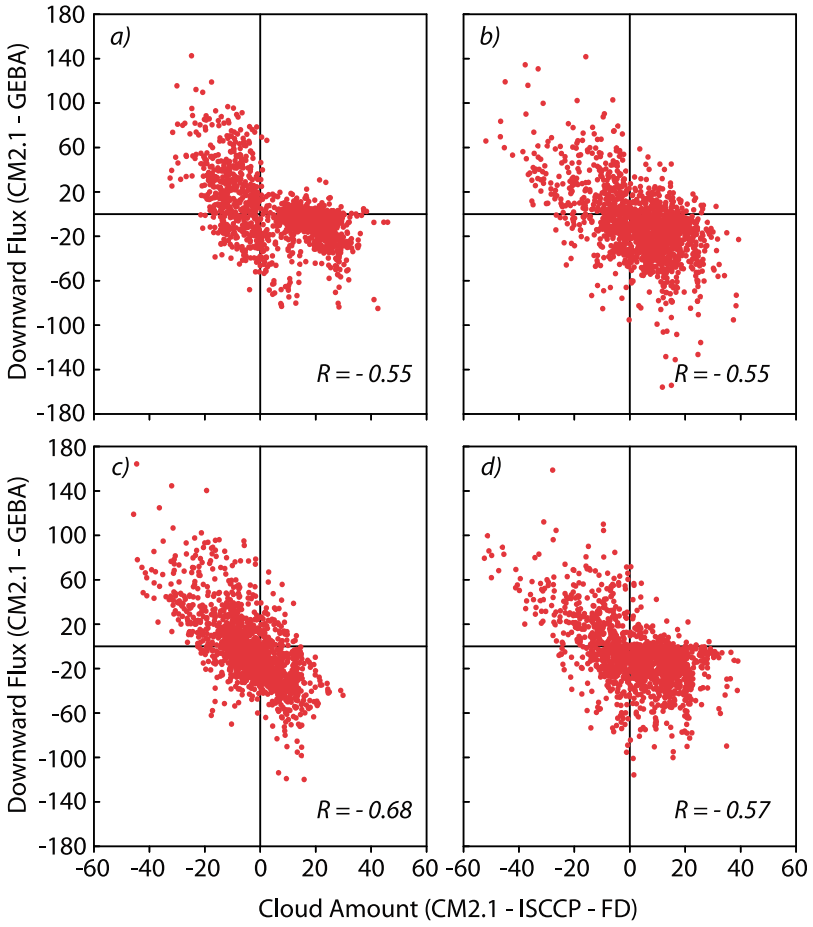

Figure 7. The relationship of the time mean CM2.1 minus GEBA downward all-sky surface flux (W/m^2) and the CM2.1 minus ISCCP-FD total cloud amount (%) at GEBA site locations over continental interiors for (a) December plus January plus February, (b) March plus April plus May, (c) June plus July plus August, and (d) September plus October plus November. Also shown is the pattern correlation coefficient R.

model's surface temperature biases, in section 4.3). Figure 7 illustrates the monthly differences partitioned into the various seasons. A correlation of between −0.5 and −0.7 is noted among all seasons. Similar to the previous analysis, this demonstrates that there is a modest degree of linkage between the shortwave surface flux and cloud amount biases. The degree of similarity in their correlation patterns (comparing Figures 6 and 7) gives a measure of confidence in using the ISCCP-FD cloud amounts as a comparative reference, for assessing the model's flux-cloud amount linkages globally.

[26] Third, the ISCCP-FD seasonal-mean cloud amounts are compared with the Long-estimated climatology, in order to ascertain the sign and magnitude of the biases between them (see Table 2). The ISCCP-FD cloud amount overestimates the BSRN value at most site locations and in all seasons. The largest overestimates (up to 30%) occur at the site location of Desert Rock; overestimates >10% occur at other site locations in western North America (Billings, Boulder, Fort Peck and Regina; see Figure 1) for most of or throughout the year. Similar biases are noted at the Southern Hemisphere sites of De Aar and Lauder. The negative biases in summer for Barrow, Ny Alesund and the South Pole sites are consistent with deficiencies in the ISCCP-FD estimation of cloud amount for polar regions [*Rossow and Schiffer*, 1999]. However, the majority of the site locations are within 15% of the BSRN value for most of or throughout the year. Thus, this analysis adds a measure of confidence in using the ISCCP-FD cloud amount climatology as a comparative reference, for assessing CM2.1's regional cloud amount biases throughout the globe.

[27] Finally, before using the ISCCP-FD flux climatology for a regional analysis of the model biases, the global pattern correlation is assessed between the model flux biases relative to it, and those relative to BSRN and GEBA values, respectively. These coefficients are listed in Table 3 and range from 0.66 to 0.76 for the different seasons. In the assessment of the model's flux biases, this demonstrates that a modest degree of consistency exists globally with respect to all three data sets, despite the fact that the ISCCP-FD results rely on radiative transfer modeling [*Zhang et al.*, 2004]. This also adds a measure of confidence toward use of the ISCCP-FD flux climatology, for assessing CM2.1's regional flux biases throughout the globe.

[28] With these results in mind, the regional patterns of CM2.1's flux and cloud amount biases, and the linkages

Table 2. Seasonal Mean Difference in the Total Cloud Amount (%) Between ISCCP-FD and the Long-Estimated Value Derived From the BSRN Data[a]

Site	Winter	Spring	Summer	Autumn
Alice Springs	12.8	3.9	6.9	13.9
Barrow	-	0.3	−12.4	−13.4
Bermuda	1.7	−1.3	−2.7	1.8
Billings	14.0	15.2	6.3	10.8
Bondville	7.8	9.9	−1.2	7.7
Boulder	12.9	10.3	10.2	11.8
Carpentras	9.6	10.3	9.2	7.7
Darwin	8.7	0.3	3.5	−0.5
De Aar	18.3	10.7	9.8	18.7
Desert Rock	16.8	30.0	27.5	21.5
Florianopolis	3.8	8.8	7.3	0.3
Fort Peck	21.9	13.7	16.2	15.6
Georg Von Neumayer	9.8	4.8	-	8.8
Goodwin Creek	10.2	8.0	−6.6	4.5
Kwajalein	7.5	5.8	9.2	12.8
Lauder	12.2	15.8	8.2	10.6
Lindenberg	−1.5	0.6	2.7	−0.5
Manus	4.5	3.3	1.6	1.9
Nauru Island	5.1	3.0	5.3	5.3
Ny Alesund	-	16.2	−6.8	-
Payerne	−7.4	5.0	7.2	−5.9
Regina	17.3	9.1	10.4	13.1
Rock Springs	−0.8	4.9	−4.1	1.6
Solar Village	−2.4	−7.4	−5.6	−1.6
South Pole	−7.2	-	-	−11.0
Syowa	14.1	1.2	-	9.2
Tamanrasset	6.3	−8.7	−15.6	−0.2
Tateno	24.4	2.0	−3.9	1.3
Toravere	-	6.8	0.9	−2.1

[a]For comparison with BSRN, the ISCCP-FD climatology is obtained for the same period as when data are available for each site location, through 2003. Missing values are due to the unavailability of a Long-determined estimate.

between them, are investigated. A regional pattern correlation coefficient is computed between the time mean (1984–2003) simulated minus ISCCP-FD flux, and the corresponding simulated minus ISCCP-FD cloud amount. This is performed using all the grid points in each 10° × 10° square domain. The method is found to be sufficient in both determining a representative value of the correlation for the domain, and in discretizing the regional dependence of the correlation around the globe. Regions exhibiting a sizable negative correlation between them (particularly <−0.7), based on this correlation analysis, are highlighted.

[29] CM2.1's seasonal mean flux differences with respect to GEBA and ISCCP-FD are illustrated in Figures 8–11, while the corresponding values with respect to the BSRN sites are listed in Table 4. Figure 12 illustrates the seasonal cloud amount differences between CM2.1 and ISCCP-FD, and Figure 13 illustrates the corresponding geographical distribution of the pattern correlation coefficient.

[30] First, the land regions exhibiting flux underestimates are highlighted. For Europe, northern and eastern Asia and North America, Figures 8–11 indicate that the model produces large biases that persist throughout the year. Compared with GEBA and ISCCP-FD, differences >10 W/m^2 encompass most of these regions, with maximum values >20 W/m^2. Further, Table 4 indicates that for the BSRN site locations of Carpentras, Payerne and Tateno, the biases can exceed 30 W/m^2. There is a distinct maximum in spring for Europe and in summer for northern and eastern Asia. Comparatively, for North America, the negative biases at the BSRN site locations are not as large, and there is also a distinct summer minimum, with more sites showing overestimates. A similar characteristic is noted in comparisons with GEBA and ISCCP-FD. In association with these flux biases, cloud amount overestimates >10% occur for these areas throughout the year, but have the least spatial coverage in summer. This characteristic is also illustrated in Figure 6 with respect to the Long-estimated cloud amounts from the BSRN data, many sites of which are in these regions (Figure 1). There, the model shows a tendency toward overestimating the cloud amounts, but less so during the summer months. Figure 13 shows that the difference patterns are negatively correlated for most of these areas; that is, flux overestimates (underestimates) are linked to cloud amount underestimates (overestimates). Thus, the model's moist bias, highlighted earlier with respect to excessive extinction by sulfate aerosols, is also associated with excessive cloud amount, resulting in the persistence of significant flux underestimates in these regions.

[31] For southern Africa (BSRN at De Aar), flux underestimates also persist throughout the year, but values >20 W/m^2 have their largest areal extent in winter and spring. For interior Australia, (BSRN at Alice Springs), there is a definitive summer maximum. These are correlated with cloud amount overestimates, and are an indication that the model can also be too moist for drier regions, especially during their driest seasons. For India, differences >30 W/m^2 occur during the summer and autumn, and are an indication that the Asian summer monsoon is likely too strong in CM2.1. Flux underestimates persist throughout the year for New Zealand (BSRN at Lauder), and occur during summer in the Arctic (BSRN at Barrow and Ny Alesund). In both cases, the features are correlated with cloud amount overestimates.

[32] Flux overestimates for land areas exceed 30 W/m^2 for equatorial Africa during the summer, and for the Amazon region during the summer and autumn. These are associated with significant cloud amount underestimates (>20%), although the patterns are correlated better for the Amazon region. This is indicative of the fact that CM2.1 does not account well for the seasonal shift in the ITCZ, producing too little precipitation for these regions [*Delworth et al.*, 2006]. In northern Australia (BSRN at Darwin), flux overestimates occur in all seasons except spring. The largest biases in both flux (especially BSRN; Table 4) and cloud amount (>10%) occur in autumn. For the remaining coastal regions of Australia, they are largest in summer and autumn, and show a good correlation with cloudiness. For southern Asia, they are noted throughout the year, with values

Table 3. Pattern Correlation Coefficient, for Each Season, Between CM2.1's All-Sky Flux Bias With Respect to BSRN and GEBA Climatology, and CM2.1's All-Sky Flux Bias With Respect to ISCCP-FD Climatology, Interpolated to the Geographical Coordinates of the BSRN and GEBA Site Locations, Respectively

	Winter	Spring	Summer	Autumn
CM2.1–BSRN versus CM2.1 – ISCCP-FD	0.67	0.71	0.72	0.73
CM2.1–GEBA versus CM2.1 – ISCCP-FD	0.76	0.71	0.66	0.70

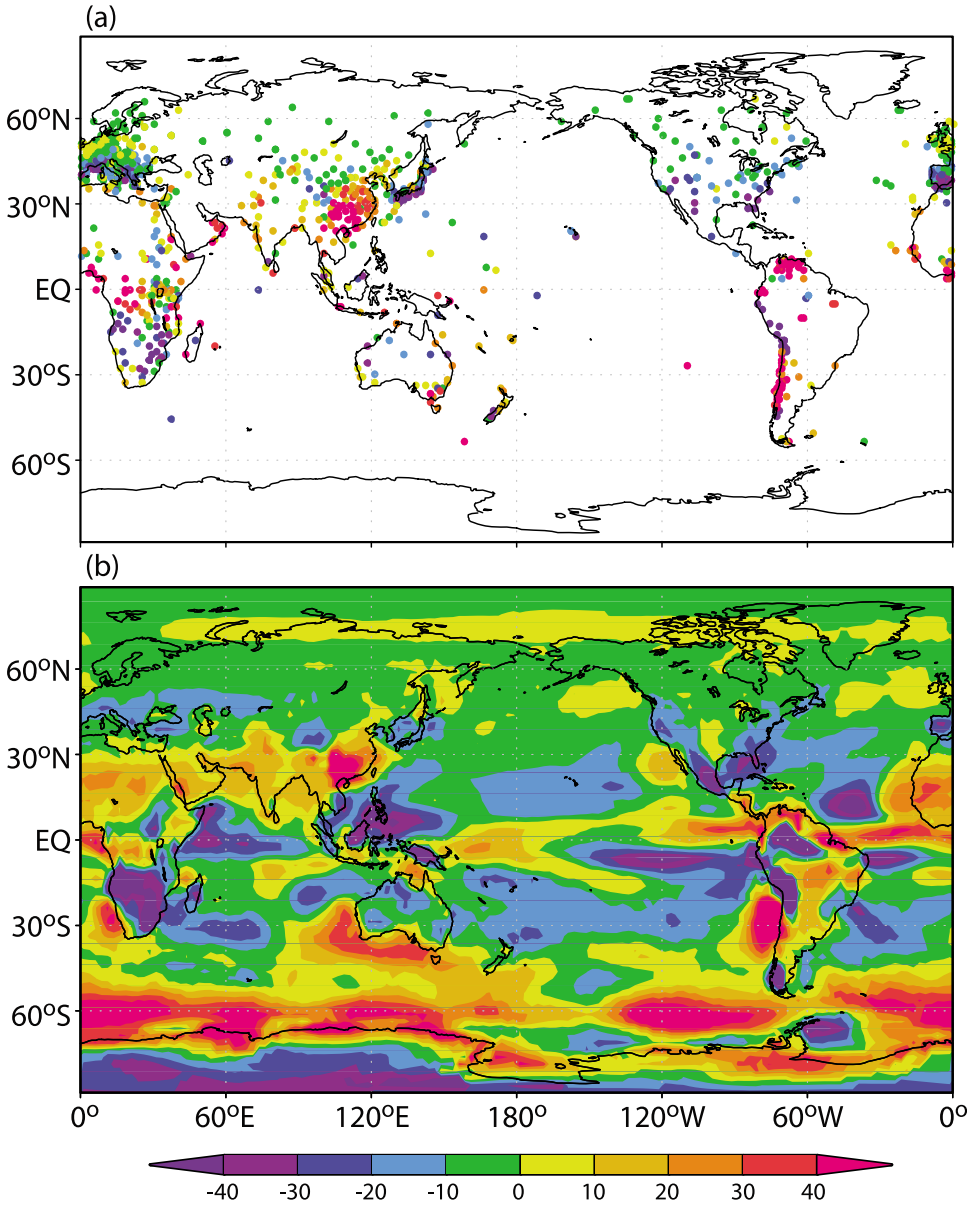

Figure 8. The Northern Hemisphere winter difference in the all-sky downward surface flux (W/m^2) between CM2.1 and the (a) GEBA climatology and (b) ISCCP-FD climatology.

>30 W/m^2 occurring in various locations for each season, and are associated with overestimates in cloud amount. For the Arctic, flux overestimates are seen to occur during spring (BSRN at Ny Alesund), and can exceed 20 W/m^2 with respect to ISCCP-FD (Figure 9). Comparisons with ISCCP-FD also indicate that this bias is present throughout the region. However, there are also accompanying cloud amount overestimates (Figure 12b), resulting in large positive correlations (Figure 13b).

[33] The occurrence of large positive correlations in the high latitudes in Figure 13 may be due in part to the difficulties associated with satellite-derived cloudiness over highly reflecting surfaces [*Rossow and Schiffer*, 1999]. For Ny Alesund, the ISCCP-FD cloud amount overestimates the long-estimated spring value by >15% (see Table 2). This results in a low bias for the ISCCP-FD downward flux, and a corresponding high bias for CM2.1, with respect to the ISCCP-FD value there. Illustrating this point, the model's flux difference with respect to the BSRN site of Ny Alesund is about 4 W/m^2 (Table 4) and <10 W/m^2 with respect to the GEBA site there (Figure 9a), but it is >20 W/m^2 with respect to ISCCP-FD in that region (Figure 9b). For this one location, if the ISCCP-FD cloud amount were in better agreement with the Long-estimated value, it would lead to a larger overestimate of cloud amount by CM2.1 than that depicted in Figure 12b. Also, it would lead to a higher value of the ISCCP-FD flux estimate, and, in turn, a smaller overestimate by CM2.1 than that depicted in Figure 9b. Assuming these conditions are true more generally for the Arctic, this outcome would, in turn, reduce the large positive correlation there (Figure 13b). This issue may play a role in the large positive correlations noted elsewhere, and in other seasons, at the high latitudes.

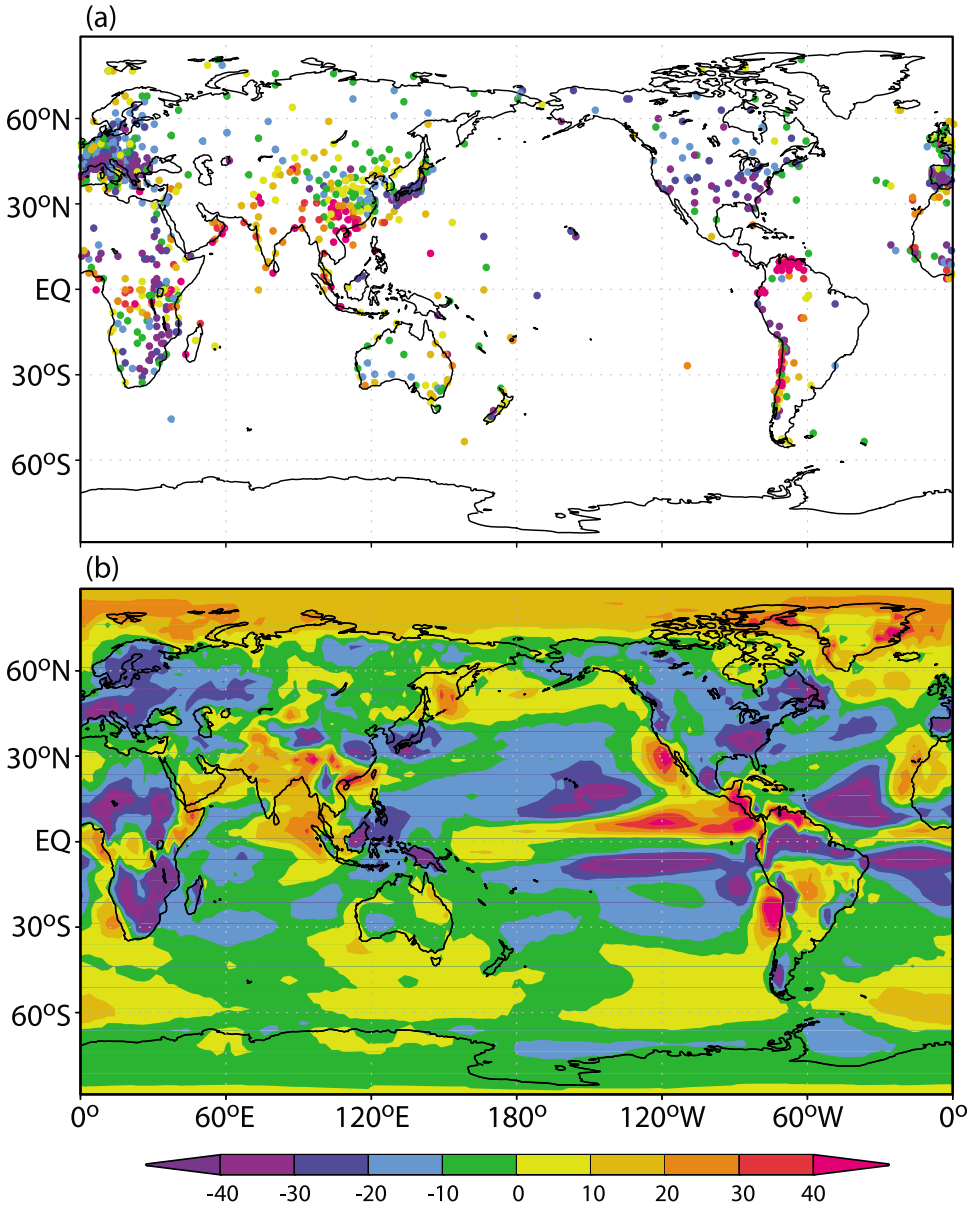

Figure 9. (a, b) Same as Figure 8 except for spring.

[34] For oceanic regions, the pattern of flux underestimates in the subtropical Pacific and Atlantic, and overestimates near and along the equator (BSRN at Manus and Nauru Island) generally persist throughout the year. These signatures also bear a linkage to cloud amount for these regions. The large biases just south of the equator are again indicative of a double ITCZ produced by CM2.1. The flux overestimates off the west coast of the Americas persist throughout the year, owing to a lack of marine stratocumulus. In the northern high latitudes, flux underestimates >30 W/m^2 occur for the North Pacific and Atlantic during summer. Overestimates occur across the southern ocean from around 60°S southward to coastal Antarctica during the summer (BSRN at Syowa). These biases are mostly correlated with cloudiness.

[35] It is acknowledged that differences in other cloud parameters (i.e., optical depth and single scattering properties) as well as the method of parameterizing shortwave radiation can also affect the flux differences between CM2.1 and ISCCP-FD, and can play a role in the bias analysis. Overall, from Figure 13, the patterns of CM2.1's flux and cloud amount biases are strongly linked over most of the globe. Thus, from this assessment and with respect to the BSRN, ISCCP-FD and GEBA climatology, it is evident that cloud amount is a climate variable for which better agreement needs to be obtained for improved simulation of the reference surface flux climatology.

4.3. Impact of Flux Biases on CM2.1 Surface Temperatures

[36] Heretofore, we have investigated how biases in CM2.1's determination of aerosol optical depth and cloud amount have resulted in differences between the simulated and observed or satellite-based estimated downward surface

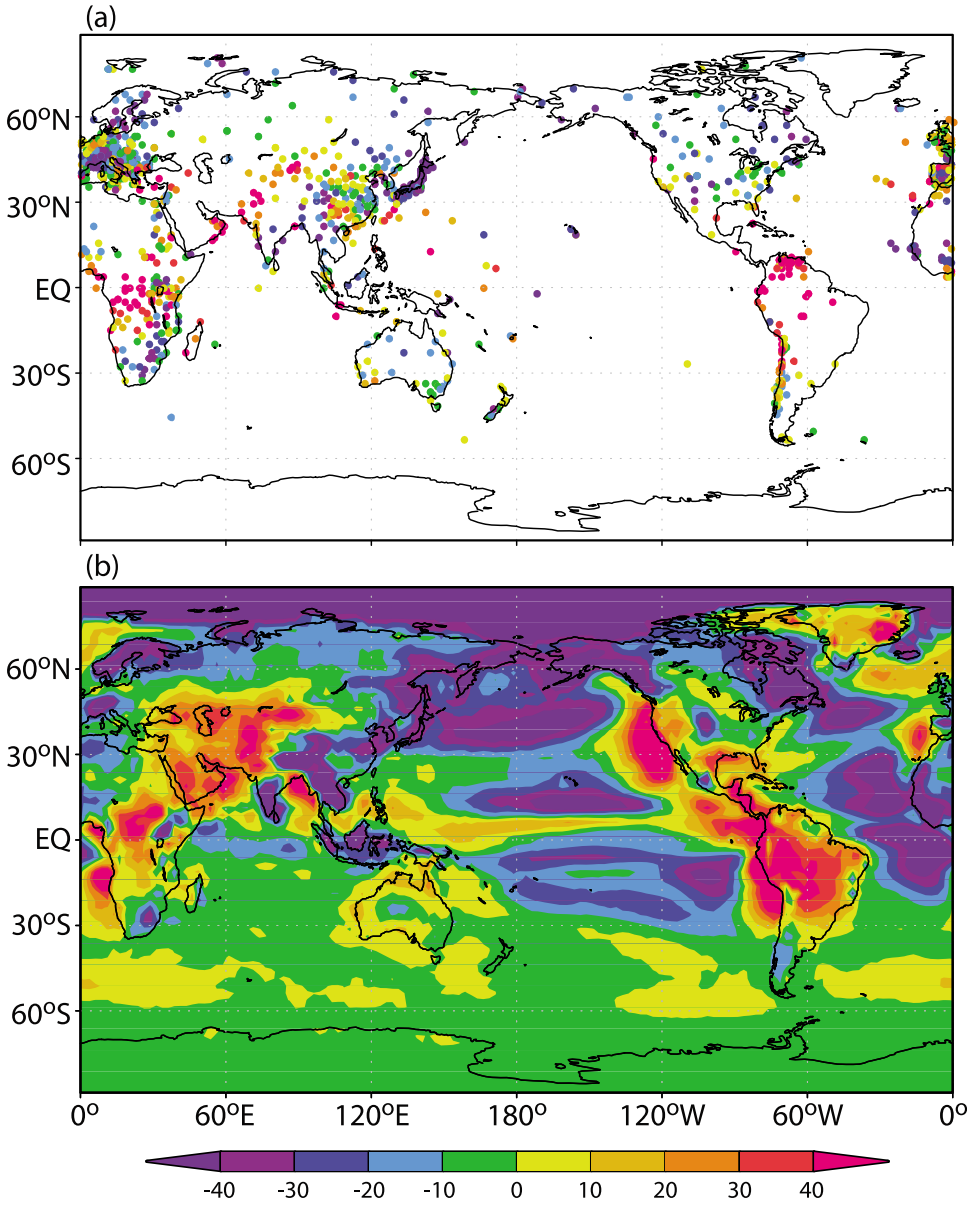

Figure 10. (a, b) Same as Figure 8 except for summer.

flux. Of additional importance is the impact that the resulting flux biases have on CM2.1's simulation of surface temperature. Simulated processes such as the formation and depletion of sea ice and hydrological cycle rely on accurate representation of the surface temperature. Proper representation of the downward solar flux at the surface is a key element toward this goal.

[37] First, the linkage between CM2.1's flux differences, and its surface temperature differences, is analyzed. The ECMWF ERA-40 surface temperature climatology, and the ISCCP-FD and GEBA flux climatology are utilized as references in this analysis. As in section 4.2, the aim is to highlight where and to what degree the two quantities are related, when examining the temporal mean fields. Second, to investigate the impact of aerosols on surface temperature, an examination is made as to what degree a reduction of CM2.1's overestimate of aerosol optical depth, arising owing to hygroscopic sulfate growth assumptions, has on reducing the surface temperature biases.

[38] As with the analysis in section 4.2, a regional pattern correlation coefficient is determined between the temporal mean flux differences with respect to ISCCP-FD climatology, and the corresponding temperature differences with respect to the ECMWF ERA-40 climatology. This is performed in order to identify the regions for which both flux and surface temperature biases are of the same sign (viz., positive correlation values). Figure 14 illustrates the seasonal surface temperature differences, and Figure 15 illustrates the correlation of the surface temperature difference with the flux differences averaged on a 10° × 10° domain (the same domain shown in Figure 13). Figure 14 also highlights areas where the temperature differences exceed twice the standard deviation of the variability, considering the model's five ensemble member integrations for this

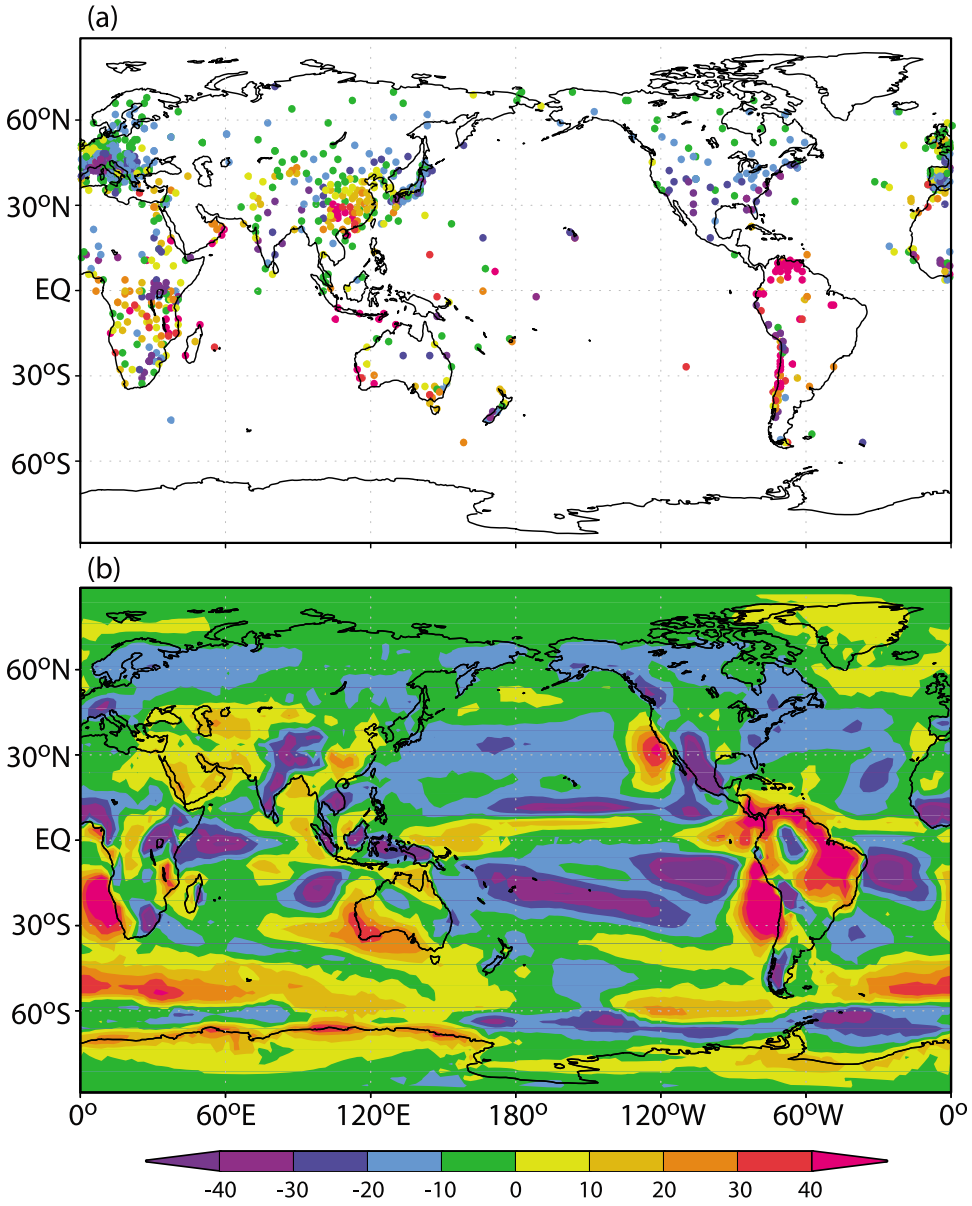

Figure 11. (a, b) Same as Figure 8 except for autumn.

period. The focus here is mainly on the regions where statistical significance, as defined above, is obtained.

[39] For North America, Europe and northern and eastern Asia, CM2.1's surface temperatures are generally biased cooler, accompanying the deficit in surface insolation. The largest magnitudes (>4 K) occur for northern and eastern Asia and North America. Similar to the flux biases, there is a distinct maximum in the cool bias in spring for Europe and a minimum in summer for North America. However, there is an excessively cold bias for northern Asia, during winter and spring. As pointed out by *Delworth et al.* [2006], a deficit of solar insolation there in winter leads to a buildup of too much ice and snow, and too high a surface albedo, which further retards the warming during spring. From this study, this higher surface albedo impacts the expected linkage between biases in the shortwave flux and the surface temperature, and, instead, contributes toward the prevalence of large negative correlations in this region during winter and spring. The largest temperature overestimate occurs for the Amazon region, in association with the excess surface insolation, especially in summer and autumn, with maximum values >6 K. The flux underestimates throughout the year for southern Africa are also well correlated with the temperature deficits there. For the Australian continent, the highest degree of correlation is evident in coastal regions during winter, with a warm bias in association with flux overestimates there. Likewise, for India and nearby parts of Asia, the highest degree of correlation occurs in summer and autumn, in association with excess monsoonal related cloudiness, leading to flux and temperature underestimates. However, the flux overestimates for equatorial Africa, especially in summer, do not show any meaningful associated warming signature.

[40] For oceanic regions, the most outstanding feature is the cooler summer bias, with maximum values >2 K for the

Table 4. Annual Mean and Seasonal Mean Difference in the Downward All-Sky Shortwave Flux (W/m^2) at the Surface Between CM2.1 and BSRN[a]

Site	Annual	Winter	Spring	Summer	Autumn
Alice Springs	−11.2	−4.2	−10.8	−27.5	−2.2
Barrow	−6.6	1.5	−13.1	−17.7	2.9
Bermuda	0.7	−14.2	−0.2	22.9	−5.5
Billings	−14.7	−5.5	−30.6	−10.5	−11.9
Bondville	−13.5	−9.0	−22.0	−5.2	−17.8
Boulder	−7.2	−10.5	−0.2	−9.1	−9.1
Carpentras	−51.8	−35.7	−68.5	−60.9	−42.0
Darwin	26.2	31.2	2.3	19.0	52.3
De Aar	−16.4	−21.2	−21.1	−19.0	−4.3
Desert Rock	−19.5	−28.4	−29.8	3.4	−23.2
Florianopolis	17.4	46.6	−17.6	14.2	26.3
Fort Peck	−6.5	−10.3	−12.5	4.5	−7.4
Georg von Neumayer	9.9	26.0	−0.3	−1.1	14.9
Goodwin Creek	−10.3	−11.5	−30.5	12.4	−11.6
Kwajalein	−0.3	−2.4	−4.3	4.8	0.9
Lauder	−14.6	−16.0	−13.4	−5.3	−23.8
Lindenberg	−14.5	−5.9	−24.1	−14.0	−14.0
Manus	27.9	40.3	20.4	14.4	36.4
Nauru Island	30.8	35.9	23.7	31.1	32.6
Ny Alesund	−1.7	−0.2	4.4	−9.4	−1.2
Payerne	−28.9	−10.0	−37.2	−47.4	−21.0
Regina	−6.7	−11.0	−15.8	8.7	−9.0
Rock Springs	−15.0	−12.1	−23.4	−1.8	−22.8
Solar Village	0.3	9.3	−16.8	6.8	2.1
South Pole	−3.6	−14.8	0.0	0.0	0.3
Syowa	6.7	15.2	0.7	−1.2	11.9
Tamanrasset	−5.0	2.3	−20.1	2.0	−4.4
Tateno	−25.6	−26.9	−31.7	−38.3	−5.6
Toravere	−14.5	−1.2	−22.9	−18.2	−15.6

[a]For comparison with BSRN, the model climatology is obtained for the same period as when data are available for each site location through 2003 (the last year of the model integration).

North Pacific, and, to a lesser extent, for the North Atlantic. These are associated with flux underestimates (Figure 10), and a high degree of correlation exists there (Figure 15c). This yields an earlier and more prolonged cooling season resulting in excessive growth of sea ice, illustrated previously with regard to the clear-sky diffuse flux overestimates at Barrow and Ny Alesund (see Figure 3). Contrastingly, a warm bias with maximum values >4 K is noted in all seasons in the southern oceans, which maximizes during the Southern Hemisphere summer. This is in association with the increased solar insolation there (Figure 8). This contributes toward a deficit in sea ice, as was illustrated earlier with regards to the clear-sky diffuse flux underestimates at Georg von Neumayer and Syowa (see Figure 3). Further, the persistence of a warm bias throughout the year off the west coast of the Americas is correlated with the flux overestimates there, due to the lack of marine stratocumulus. Elsewhere, the temperature biases for oceanic regions are not strongly positively correlated with the flux biases nor are statistically significant. Overall, land areas show more of a positive correlation between the flux and surface temperature biases. These are reflections of the fact that, unlike land areas where temperatures tend to respond more locally and quickly to the incoming insolation, sea surface temperatures tend to respond far more slowly to changes in insolation, owing to the large thermal inertia of the water. This may also partly explain why strong negative correlations can also occur over oceanic locations as seen in Figure 15.

[41] Similar to the methodology described for Figure 7, Figure 16 shows a scatterplot of the model's flux differences with GEBA climatology, and its surface temperature differences, at the GEBA site locations. A positive correlation is noted in each season, with the least occurring in winter and the most in summer. This demonstrates from a land-only, global perspective that shortwave surface flux biases are linked to surface temperature biases. However, the highly regional nature of the dependence noted in Figure 15 results in a correlation (<0.5) that overall is weaker than its relationship with cloud amount (Figure 7).

[42] These results test the links between atmospheric constituents (chiefly aerosols and clouds) and surface fluxes and temperature. Knowledge of these links serves as an important guide for making improvements to the model's determination of cloudiness and aerosol optical depth, particularly for regional domains. For cloudiness, however, it is difficult to selectively target specific geographical regions to perform corrections in models, essentially because clouds, circulation and climate are intimately interconnected. In the present framework, the "control" integrations that yield the unperturbed state of the model involve necessary adjustment of poorly known cloud-related parameters, in order to enable a global-and-annual-mean radiative balance at the top-of-the-atmosphere consistent with present-day observations. Once such a base state of the model has been attained, the model is deployed for the perturbation integrations whose results have been analyzed here. The above tuning process is applied to the model in a global-mean sense. Thus, to reduce cloud biases, improvements are needed in the basic model assumptions affecting the formation and depletion of clouds in the globe as a whole, rather than indulging in local corrections and/or adjustments.

[43] In comparison to cloudiness corrections, regional improvements to the aerosol optical depth are relatively much easier to incorporate, as, in the context of CM2.1, the aerosols are prescribed, as opposed to interacting with the circulation. For example, the comparisons have revealed that the most prominent bias in CM2.1 is a significant overestimate of the sulfate aerosol optical depth for Europe, Asia and North America in the presence of very high humidity. Part of the problem could be the dry sulfate aerosol concentrations themselves, as simulated by the chemistry-transport model whose results are used in CM2.1 [*Horowitz*, 2006]. However, a major factor is very likely the behavior of the hygroscopicity expression describing the swelling of the sulfate aerosols at very high values of the relative humidity. A handicap here is that there is not much by way of laboratory substantiation for the behavior of the mathematical function beyond ~95% relative humidity [*Ginoux et al.*, 2006]. One practical adjustment in the climate model could be to restrict the use of the expression at high relative humidity, consistent with the limits from the laboratory measurements, and thus prevent the occurrence of unrealistic large optical depths at relative humidity exceeding say 95%.

[44] The effects of reducing the aerosol-related hygroscopic bias is illustrated here, by utilizing an ensemble of CM2.1 model experiments performed to address this issue. These experiments constrain the sulfate aerosol optical

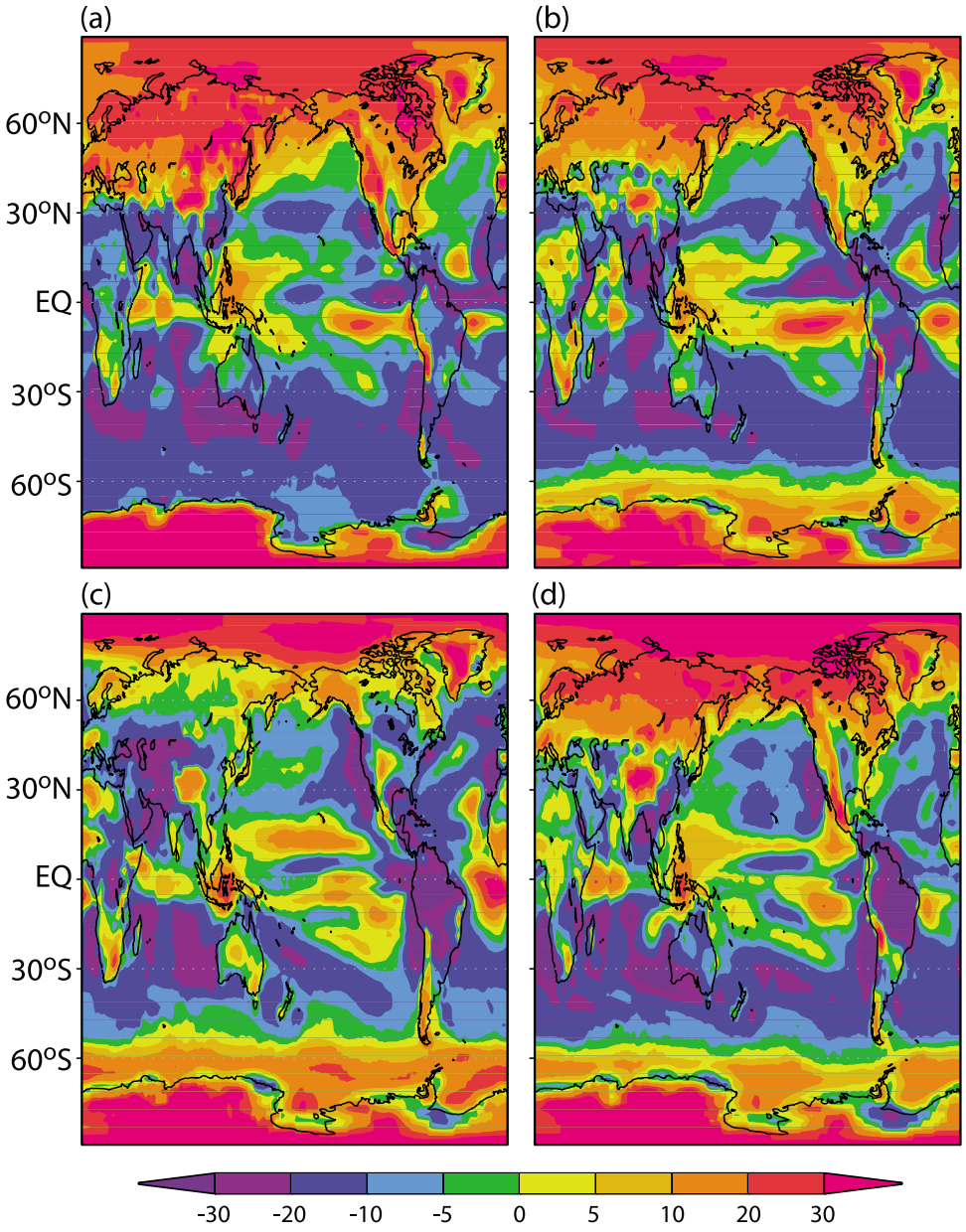

Figure 12. The difference in the total cloud amount (%) between CM2.1 and ISCCP-FD climatology (base period 1984–2003) for (a) winter, (b) spring, (c) summer, and (d) autumn.

properties to be entirely nonhygroscopic, so that the sulfate aerosol optical depth is reduced to its "dry" value (assumed here to be the value defined at 30% relative humidity). The motivation is to examine the impact of a reduction in aerosol optical depth, on the corresponding reduction in the surface temperature underestimates for key geographical regions, relative to the results obtained above for the nominal hygroscopic case. It is cautioned that this exercise is done for diagnostic purposes only, and is not meant as a plausible implementation in an operational model.

[45] To illustrate the reduction that occurs, the model's present-day monthly mean aerosol optical depth for the nonhygroscopic case is first compared against the hygroscopic case, and the AERONET values at and near the BSRN site locations (see Figure 5). There are significant reductions evident for the European, Asian and North American sites. This brings the model values into much better apparent agreement with the AERONET climatology there. Second, the global distribution of the magnitude of the historical-mean reduction in the present-day aerosol optical depth, with respect to the hygroscopic case, is illustrated in Figure 17a. The largest reduction in the aerosol optical depth (>0.2) occurs for Europe, Asia and eastern North America, as may be expected from the discussion in section 4.1.

[46] The corresponding difference obtained in the surface temperature, between the nonhygroscopic and hygroscopic cases, is illustrated in Figure 17b. There is generally an increase in surface temperature, in view of sulfate's global

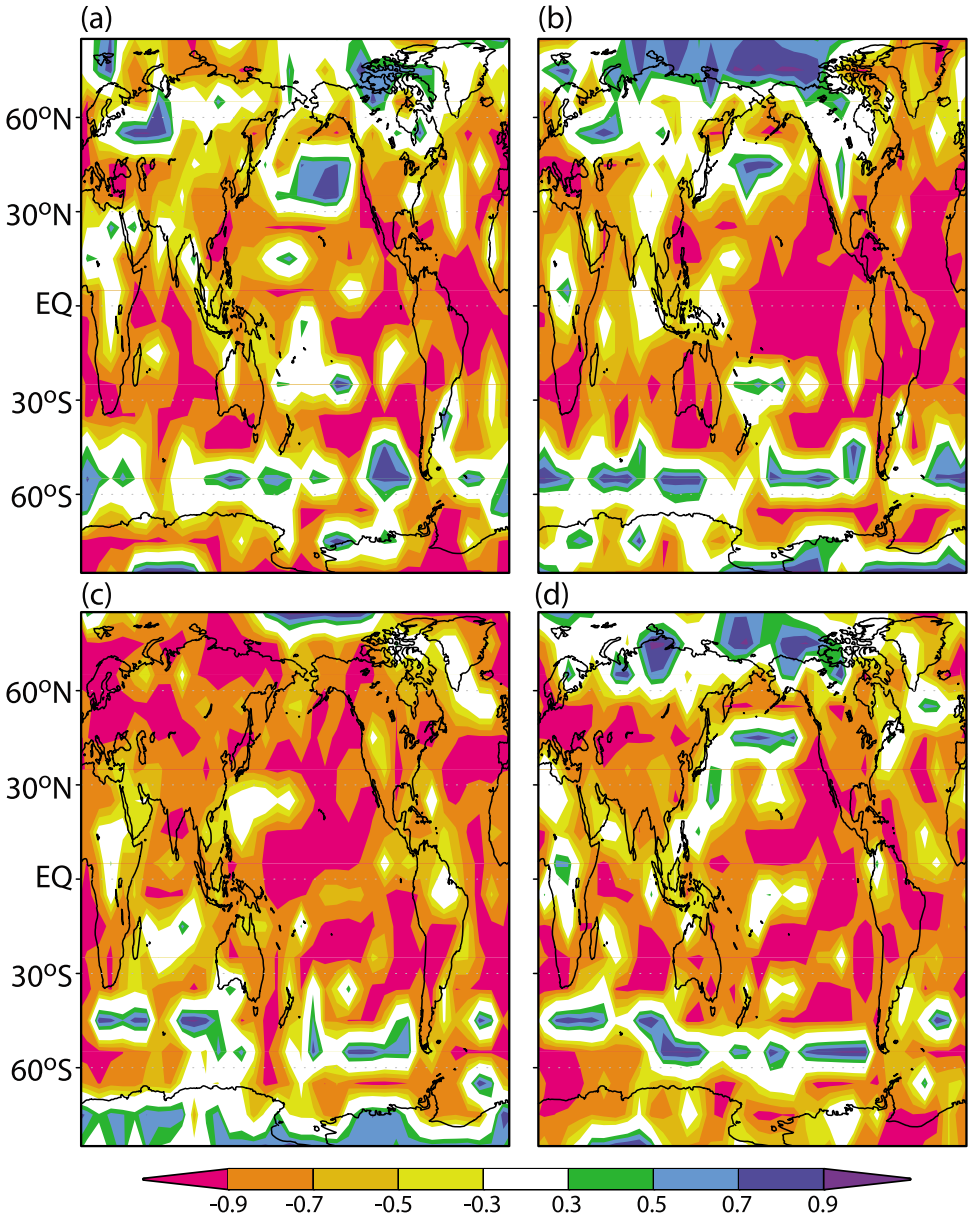

Figure 13. The pattern correlation coefficient between the time mean (1984–2003) CM2.1 minus ISCCP-FD downward surface flux and the CM2.1 minus ISCCP-FD total cloud amount for (a) winter, (b) spring, (c) summer, and (d) autumn. Results are obtained using the grid point values in each 10° × 10° square domain. Only values of magnitude >0.3 are shown.

contribution in the model. But for the key Northern Hemisphere land areas, and in particular a large part of Asia and eastern North America, increases of a degree or more occur. The difference in the surface temperature between the hygroscopic case and ECMWF ERA-40 climatology is illustrated in Figure 17c. Superimposing the temperature increases noted in Figure 17b onto the differences in Figure 17c amounts to a 10–30% reduction of the cold biases present for these regions, relative to the hygroscopic case. In spite of this, however, significant underestimates (>2 K) exist.

[47] The resulting surface temperature increases confirm that aerosol optical depth biases (in the form of overestimates) impact the surface temperature bias, by affecting the radiative component of the surface heat budget. It is anticipated that temperature increases of this magnitude would occur in future model improvements that address the aforementioned aerosol and its humidification issues, and produce aerosol optical depths consistent with observed AERONET values in these regions. However, it is evident that the effect of improving the simulation of aerosol optical depth on the surface temperature simulation is limited; refinement in the simulation of cloudiness in the model will likely lead to more substantial improvements in simulating the surface temperature in these regions (and globally in general). It should also be noted that CM2.1 does not con-

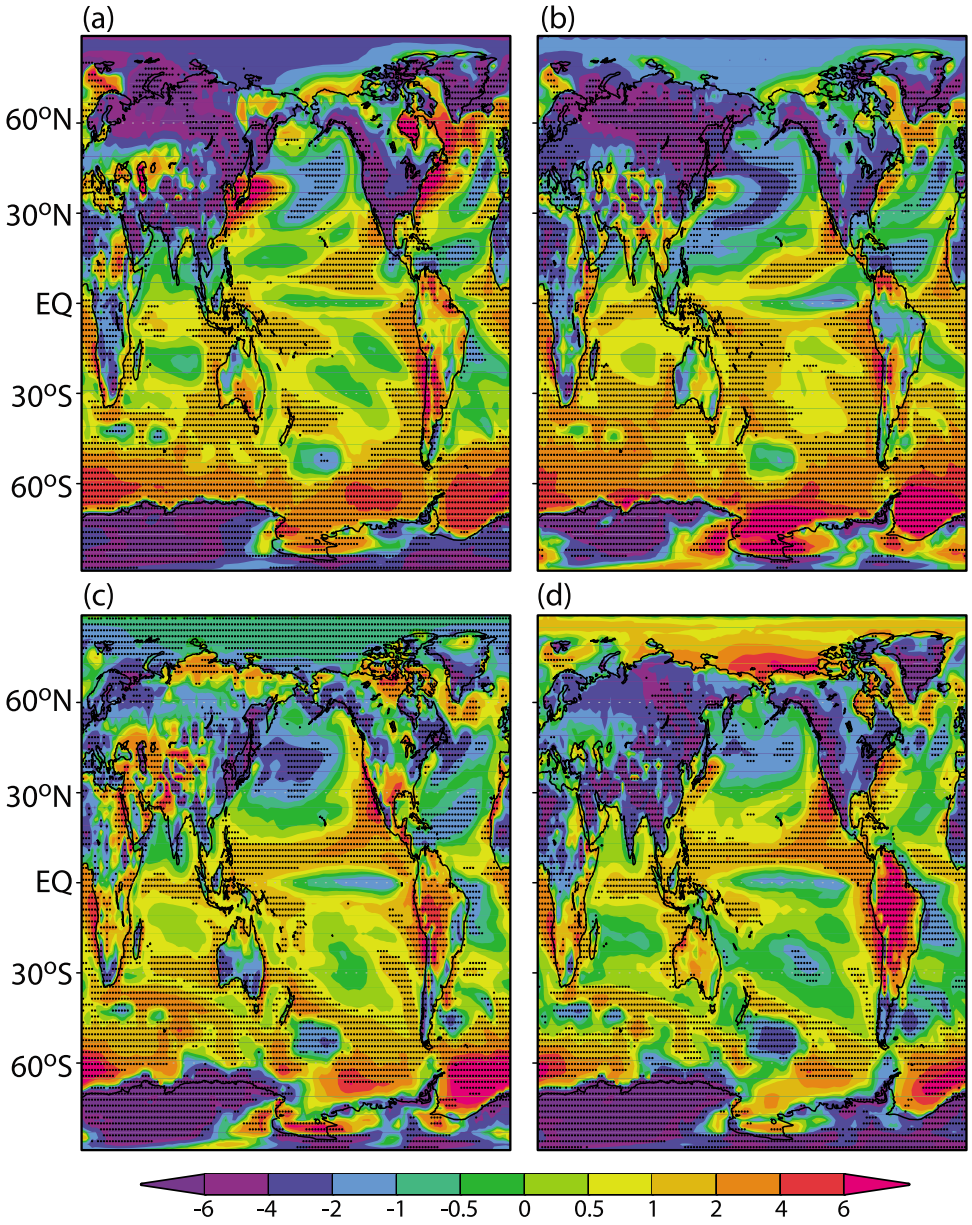

Figure 14. The difference in the surface temperature (K) between CM2.1 and European Centre for Medium-Range Weather Forecasts (ECMWF) ERA-40 climatology (base period 1984–2003) for (a) winter, (b) spring, (c) summer, and (d) autumn. Regions where the differences exceed twice the standard deviation of the model's variability for this period are stippled.

sider the interactions of aerosols with clouds. This could have additional impacts on the analyses done in this study.

5. Conclusions

[48] In this study, we have used results from the GFDL coupled model (CM2.1) experiments to examine the spatial patterns of the differences between model-simulated, and both observed and estimated downward shortwave flux climatology at the surface, for clear-sky and all-sky atmospheres. The monthly mean clear-sky flux climatology derived from the BSRN data set has been shown to be a useful tool in demonstrating model biases in aerosol optical depth, through comparisons with observed data. The model locations corresponding to the European, Asian and North American sites display a large underestimate in the direct, and overestimate in the diffuse, leading to an underestimate in the total clear-sky flux (maximum monthly magnitudes of >40, 20 and 20 W/m^2, respectively). These differences are accompanied by an overestimate in aerosol optical depth (owing to sulfate aerosol) relative to AERONET data in the vicinity of these sites. Contrastingly, the flux differences are reduced but are of similar sign in lower latitudes, specifically at the sites of Darwin, Florianopolis and Nauru Island, in conjunction with an underestimate in aerosol optical depth. CM2.1 underestimates of carbonaceous aerosols in

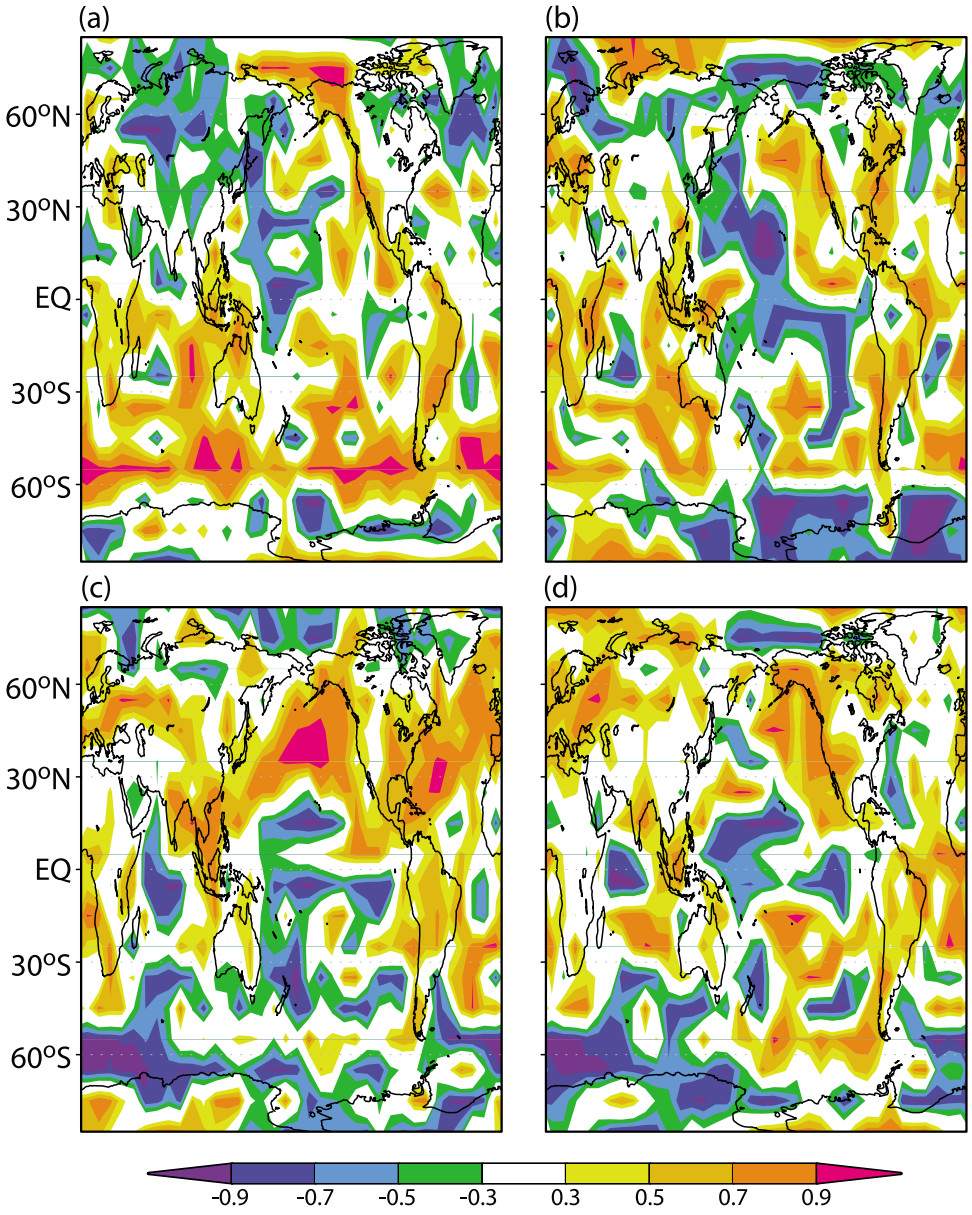

Figure 15. The pattern correlation coefficient between the time mean (1984–2003) CM2.1 minus ISCCP-FD downward surface flux and the CM2.1 minus ECMWF ERA-40 surface temperature for (a) winter, (b) spring, (c) summer, and (d) autumn. Results are obtained using the grid point values in each 10° × 10° square domain. Only values of magnitude >0.3 are shown. For ease of comparison, the color legend is the reverse of that from Figure 13.

regions of biomass burning, or in sea-salt concentrations at oceanic sites, are contributing factors at these locations. Underestimates in the diffuse flux at polar site locations highlight deficiencies in the modeling of sea ice. This result also demonstrates the usefulness of the derived clear-sky climatology from the BSRN observations.

[49] The differences between CM2.1 and the BSRN, GEBA and ISCCP-FD surface fluxes have been analyzed to establish the sign and magnitude of the all-sky flux biases. An investigation has also been made of the linkage of these flux biases to those in the model's simulated cloud amounts. Model comparisons have been made with the BSRN flux climatology and the Long-estimated cloud amounts; also, comparisons have been performed with the GEBA flux climatology and the ISCCP-FD cloud amounts. There is a modest degree of negative correlation between the flux and cloud amount biases. Further, the ISCCP-FD flux and cloud amount data have been used together as a reference for quantifying the regional pattern of this relationship. With respect to all three data sets, the largest flux underestimates occur for Europe, Asia and North America. These generally persist throughout the year, but have their greatest areal extent and magnitude during the spring and autumn seasons. For the North Pacific and North Atlantic, a large flux underestimate occurs in summer. These are shown to be mostly related to overestimates in cloud amount. The sur-

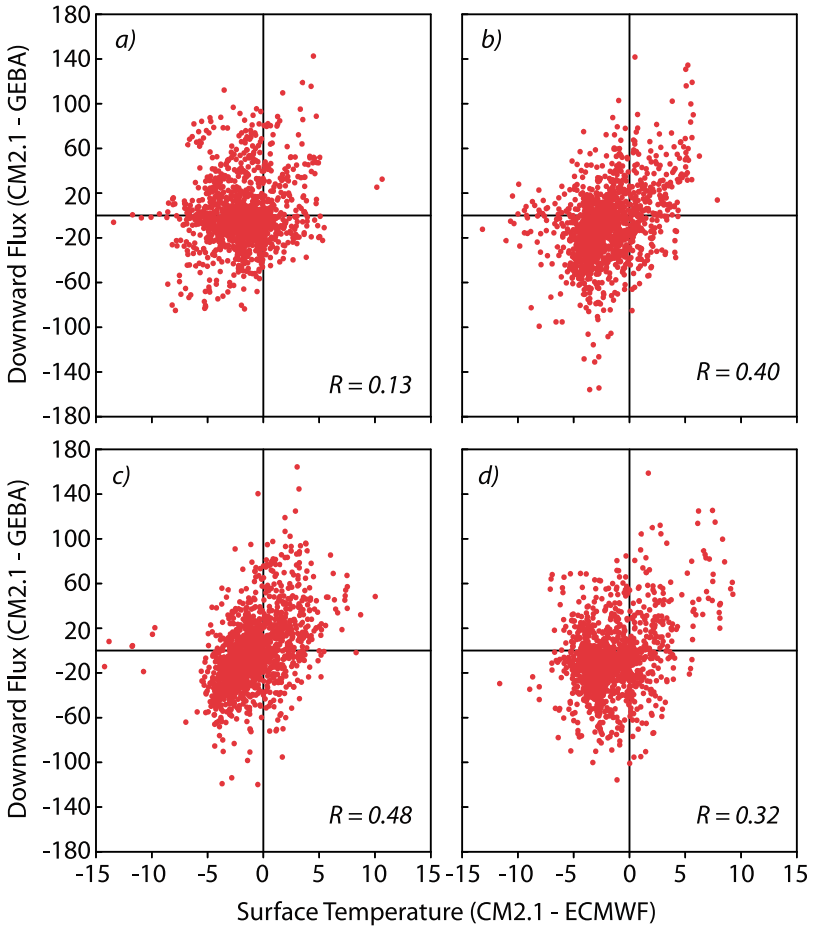

Figure 16. The relationship of the time mean CM2.1 minus GEBA downward all-sky surface flux (W/m^2) and the CM2.1 minus ECMWF ERA-40 surface temperature (K) at GEBA site locations over continental interiors for (a) December plus January plus February, (b) March plus April plus May, (c) June plus July plus August, and (d) September plus October plus November. Also shown is the pattern correlation coefficient R.

face solar flux overestimates are most pronounced for equatorial Africa during the summer, and for the Amazon region during the summer and autumn; both are associated with underestimates in cloud amount. Overall, the patterns of CM2.1's flux and cloud amount biases are strongly linked over most of the globe. Thus, the degree of the model bias in cloud amount becomes an important factor in governing the corresponding bias in the downward all-sky flux at the surface. A major exception to this relationship occurs in higher latitudes; this points out potential problems with satellite-derived cloudiness over bright surfaces there.

[50] The flux biases are correlated with colder surface temperature biases for Europe, Asia and North America, and warmer biases for the Amazon region; thus, they have a direct and substantial linkage to surface temperature biases in the continental interiors. For oceanic regions, flux underestimates for the North Pacific and North Atlantic are strongly correlated with significantly cooler biases in summer. Contrastingly, a flux overestimate that maximizes in the southern oceans during the summer season is strongly correlated with a warm bias there. These flux biases also have a significant bearing on the sea-ice climatology. Overall, this comparison exercise points out that significant shortwave flux biases at the surface affect how well the surface temperature is simulated in the model, but the degree to which it does is highly dependent on location and season.

[51] One refinement that demonstrates the effect of reducing the bias in the sulfate aerosol optical depth is the assumption of nonhygroscopicity in the model. A "dry" sulfate aerosol simulation reduces the overestimate of aerosol optical depth for Europe, Asia and North America. The resulting surface temperature increases partially offset the underestimates seen in the simulation done with the hygroscopic sulfate assumption. It is cautioned, though, that the "dry" sulfate model simulation performed here may be erring overly in reducing the actual optical depth by an exaggerated amount. Also, the fact that sulfate concentrations may be underestimated, likely is a minor, but non-negligible, contributing factor. The principal point is that sulfate optical depth at extremely high relative humidity (close to 100%) is overestimated in CM2.1. Improvements to be undertaken in the future should include addressing the representation of hygroscopicity in the presence of very high relative humidity, and accounting for additional complexities such as internal mixtures of aerosol species. With these improvements, further reduction of both aerosol and surface

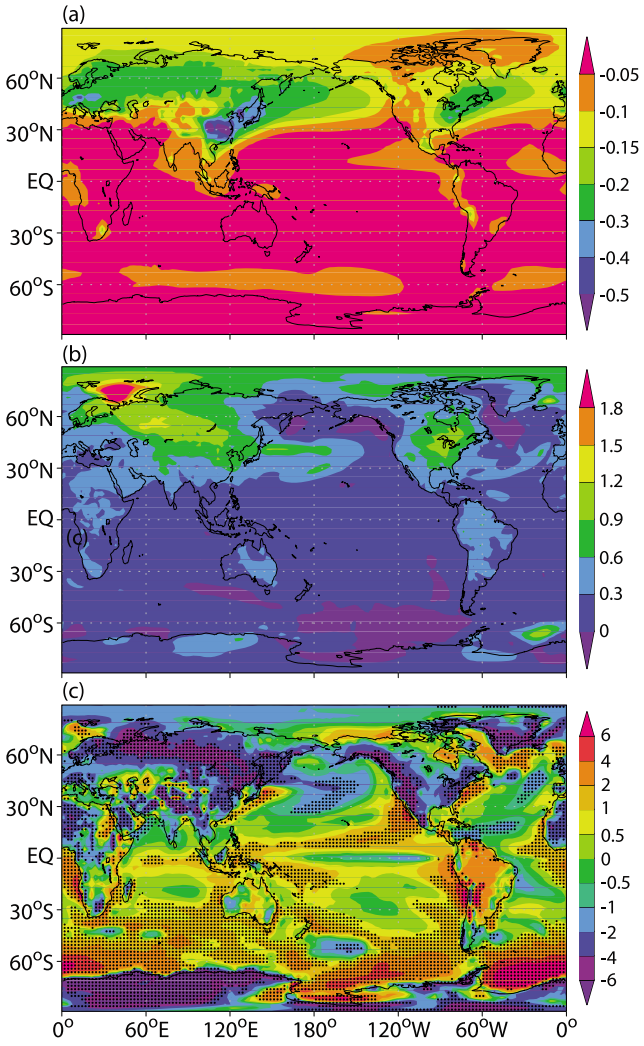

Figure 17. The time mean (1984–2003) difference in the (a) aerosol optical depth and (b) surface temperature, between an ensemble of CM2.1 experiments assuming "dry" sulfate and the hygroscopic case considered in this study. (c) The time mean difference in the surface temperature (K) between the hygroscopic case considered in this study and ECMWF ERA-40 climatology. Regions where the difference exceeds twice the standard deviation of the model's variability for this period are stippled.

temperature biases can be anticipated. However, more substantial improvements in representing the surface temperature will require significant refinements in the treatment of cloudiness in the model. It should also be noted that this study has not considered the plausible additional impacts, on the bias analyses, owing to the interaction of aerosols with clouds.

[52] Two matters not previously addressed in this study are important to the conclusions reached. First of all, some issues may potentially arise with the use of coupled model simulations for the analyses performed in this study. In comparison with AMIP-type runs, that is, atmosphere-only runs where the evolution of SSTs are prescribed according to observations, the coupled models contain an additional uncertainty viz. biases in the internally computed SSTs, and potential ocean-atmosphere coupling problems. These may, in turn, introduce biases in the simulated cloud amount and water vapor distribution, and make the causes of the flux biases more difficult to interpret. In order to investigate these issues, most of the analyses done in this study were repeated using an AMIP-type experiment with the same atmospheric model as used in the coupled experiment. It is found that the globally averaged cloud amount and surface temperature are in better agreement with the reference data sets used in this study, than the corresponding quantities obtained from the coupled model. However, the flux simulation is somewhat degraded, both for clear skies (at the BSRN sites) and for all skies (globally averaged), and the simulation of surface relative humidity is not improved. The resulting correlations among the flux, cloud amount and surface temperature biases are similar or somewhat degraded compared to the coupled model results. Thus, for the analyses done in this study, the results for this uncoupled experiment do not show differences significant enough to alter the main findings stated above.

[53] Second, a more complete assessment of deficiencies in the GCM's simulation of the surface radiation budget requires comparisons with longwave reference data sets [*Wild et al.*, 2001]. Although the appropriate and detailed analyses are beyond the scope of this study, one noteworthy result found utilizing the ISCCP-FD data set is that model biases in the downward longwave flux and surface temperature are highly correlated in certain regions, and are more geographically extensive than those for the shortwave component. Thus, improvements in the global simulation of surface temperature will also require consideration of the factors contributing toward the longwave flux biases. Such analysis is also likely to point to cloud amount as an important contributing factor.

[54] The analyses done with the shortwave surface flux data sets provide a number of useful metrics for assessing how well the aerosol optical depth, sea ice, cloud amount and surface temperature are represented, and to what extent they need to be improved upon in weather and climate models. A recommendation from this study is the desirability of having climate model simulations, for example, those used in IPCC, compared in depth with the atmospheric and surface radiation-related observations, to test and subsequently improve upon the aerosol, cloud and radiation treatments, and thus reduce biases in the model simulations. Together, the improvements in simulating aerosol and cloud radiative effects, and sustained comparisons with the relevant observations, will play a large role in the improved fidelity of climate models, and eventually be useful in the practical aspect of climate prediction.

[55] **Acknowledgments.** We thank Paul Ginoux, M. D. Schwarzkopf, and two anonymous reviewers for their comments and suggestions for this manuscript.

References

Anderson, J. L., et al. (2004), The new GFDL global atmosphere and land model AM2–LM2: Evaluation with prescribed SST simulations, *J. Clim.*, *17*, 4641–4673, doi:10.1175/JCLI-3223.1.

Arking, A. (1996), Absorption of solar energy in the atmosphere: Discrepancy between model and observations, *Science*, *273*, 779–782, doi:10.1126/science.273.5276.779.

Bodas-Salcedo, A., M. A. Ringer, and A. Jones (2008), Evaluation of the surface radiation budget in the atmospheric component of the Hadley Centre Global Environmental Model (HADGEM1), *J. Clim.*, *21*, 4723–4748, doi:10.1175/2008JCLI2097.1.

Cess, R. D., et al. (1995), Absorption of solar radiation by clouds: Observations versus models, *Science*, *267*, 496–499, doi:10.1126/science.267.5197.496.

Delworth, T. L., et al. (2006), GFDL's CM2 global coupled climate models. Part I: Formulation and simulation characteristics, *J. Clim.*, *19*, 643–674, doi:10.1175/JCLI3629.1.

Forster, P., et al. (2007), Changes in atmospheric constituents and in radiative forcing, in *Climate Change 2007: The Physical Science Basis. Contribution of Working Group I to the Fourth Assessment Report of the Intergovernmental Panel on Climate Change*, edited by S. Solomon et al., pp. 129–234, Cambridge Univ. Press, Cambridge, U. K.

Freidenreich, S. M., and V. Ramaswamy (1999), A new multiple-band solar radiative parameterization for general circulation models, *J. Geophys. Res.*, *104*, 31,389–31,409, doi:10.1029/1999JD900456.

Freidenreich, S. M., and V. Ramaswamy (2005), Refinement of the Geophysical Fluid Dynamics Laboratory solar benchmark computations and an improved parameterization for climate models, *J. Geophys. Res.*, *110*, D17105, doi:10.1029/2004JD005471.

Fu, Q., and K. N. Liou (1993), Parameterization of the radiative properties of cirrus clouds, *J. Atmos. Sci.*, *50*, 2008–2025, doi:10.1175/1520-0469(1993)050<2008:POTRPO>2.0.CO;2.

Garratt, J. R. (1994), Incoming shortwave fluxes at the surface: A comparison of GCM results with observations, *J. Clim.*, *7*, 72–80, doi:10.1175/1520-0442(1994)007<0072:ISFATS>2.0.CO;2.

Gilgen, H., M. Wild, and A. Ohmura (1998), Means and trends of shortwave irradiance at the surface estimated from global energy balance archive data, *J. Clim.*, *11*, 2042–2061.

Ginoux, P., L. W. Horowitz, V. Ramaswamy, I. V. Geogdzhayev, B. N. Holben, G. Stenchikov, and X. Tie (2006), Evaluation of aerosol distribution and optical depth in the Geophysical Fluid Dynamics Laboratory coupled model CM2.1 for present climate, *J. Geophys. Res.*, *111*, D22210, doi:10.1029/2005JD006707.

Haywood, J. H., and V. Ramaswamy (1998), Global sensitivity of the direct radiative forcing due to anthropogenic sulfate and black carbon aerosols, *J. Geophys. Res.*, *103*, 6043–6058, doi:10.1029/97JD03426.

Holben, B. N., et al. (2001), An emerging ground-based aerosol climatology: Aerosol optical depth from AERONET, *J. Geophys. Res.*, *106*, 12,067–12,097, doi:10.1029/2001JD900014.

Horowitz, L. W. (2006), Past, present, and future concentrations of tropospheric ozone and aerosols: Methodology, ozone evaluation, and sensitivity to aerosol wet removal, *J. Geophys. Res.*, *111*, D22211, doi:10.1029/2005JD006937.

Horowitz, L. W., et al. (2003), A global simulation of tropospheric ozone and related tracers: Description and evaluation of MOZART, version 2, *J. Geophys. Res.*, *108*(D24), 4784, doi:10.1029/2002JD002853.

Joseph, J. H., W. Wiscombe, and J. A. Weinman (1976), The delta-Eddington approximation for radiative flux transfer, *J. Atmos. Sci.*, *33*, 2452–2459, doi:10.1175/1520-0469(1976)033<2452:TDEAFR>2.0.CO;2.

Long, C. N., and T. P. Ackerman (2000), Identification of clear skies from broadband pyranometer measurements and calculation of downwelling shortwave cloud effects, *J. Geophys. Res.*, *105*, 15,609–15,626, doi:10.1029/2000JD900077.

Long, C. N., T. P. Ackerman, K. L. Gaustad, and J. N. S. Cole (2006), Estimation of fractional sky cover from broadband shortwave radiometer measurements, *J. Geophys. Res.*, *111*, D11204, doi:10.1029/2005JD006475.

Ohmura, A., et al. (1998), Baseline Surface Radiation Network (BSRN/WCRP): New precision radiometry for climate research, *Bull. Am. Meteorol. Soc.*, *79*, 2115–2136.

Ramaswamy, V., and M. M. Bowen (1994), Effects of changes in radiatively active species upon the lower stratospheric temperatures, *J. Geophys. Res.*, *99*, 18,909–18,921, doi:10.1029/94JD01310.

Rossow, W. B., and R. A. Schiffer (1999), Advances in understanding clouds from ISCCP, *Bull. Am. Meteorol. Soc.*, *80*, 2261–2287, doi:10.1175/1520-0477(1999)080<2261:AIUCFI>2.0.CO;2.

Rothman, L. S., et al. (2003), The HITRAN molecular spectroscopic database: Edition 2000 including updates through 2001, *J. Quant. Spectrosc. Radiat. Transfer*, *82*, 5–44, doi:10.1016/S0022-4073(03)00146-8.

Slingo, A. (1989), A GCM parameterization of the shortwave radiative properties of water clouds, *J. Atmos. Sci.*, *46*, 1419–1427, doi:10.1175/1520-0469(1989)046<1419:AGPFTS>2.0.CO;2.

Wild, M. (1999), Discrepancies between model-calculated and observed shortwave absorption in areas with high aerosol loadings, *J. Geophys. Res.*, *104*, 27,361–27,371, doi:10.1029/1999JD900925.

Wild, M. (2008), Short-wave and long-wave surface radiation budgets in GCMs: A review based on the IPCC-AR4/CMIP3 models, *Tellus, Ser. A*, *60*, 932–945, doi:10.1111/j.1600-0870.2008.00342.x.

Wild, M. (2009), Global dimming and brightening: A review, *J. Geophys. Res.*, *114*, D00D16, doi:10.1029/2008JD011470.

Wild, M., and B. Liepert (1998), Excessive transmission of solar radiation through the cloud-free atmosphere, *Geophys. Res. Lett.*, *25*, 2165–2168, doi:10.1029/98GL51595.

Wild, M., A. Ohmura, H. Gilgen, and E. Roeckner (1995), Validation of general circulation model radiative fluxes using surface observations, *J. Clim.*, *8*, 1309–1324, doi:10.1175/1520-0442(1995)008<1309:VOGCMR>2.0.CO;2.

Wild, M., A. Ohmura, H. Gilgen, J. Morcrette, and A. Slingo (2001), Evaluation of downward longwave radiation in general circulation models, *J. Clim.*, *14*, 3227–3239, doi:10.1175/1520-0442(2001)014<3227:EODLRI>2.0.CO;2.

Wild, M., C. N. Long, and A. Ohmura (2006), Evaluation of clear-sky solar fluxes in GCMs participating in AMIP and IPCC-AR4 from a surface perspective, *J. Geophys. Res.*, *111*, D01104, doi:10.1029/2005JD006118.

Zhang, M. H., W. Y. Lin, and J. T. Kiehl (1998), Bias of atmospheric shortwave absorption in the NCAR Community Climate Models 2 and 3: Comparison with monthly ERBE/GEBA measurements, *J. Geophys. Res.*, *103*, 8919–8925, doi:10.1029/98JD00343.

Zhang, Y.-C., W. B. Rossow, A. A. Lacis, V. Oinas, and M. I. Mishchenko (2004), Calculation of radiative fluxes from the surface to top of atmosphere based on ISCCP and other global data sets: Refinements of the radiative transfer model and the input data, *J. Geophys. Res.*, *109*, D19105, doi:10.1029/2003JD004457.

Zhang, Y., C. N. Long, W. B. Rossow, and E. G. Dutton (2010), Exploiting diurnal variations to evaluate the ISCCP-FD flux calculations and radiative-flux-analysis-processed surface observations from BSRN, ARM, and SURFRAD, *J. Geophys. Res.*, *115*, D15105, doi:10.1029/2009JD012743.

S. M. Freidenreich and V. Ramaswamy, Geophysical Fluid Dynamics Laboratory, NOAA, Princeton University, Forrestal Campus, 201 Forrestal Rd., Princeton, NJ 08540, USA. (Stuart.Freidenreich@noaa.gov)